LOK/SLK kinases and ERM proteins function together to regulate apical morphology and inhibit RhoA signaling

Riasat Zaman[1,4], Andrew Lombardo[1,4], Cécile Sauvanet[1,2], Raghuvir Viswanatha[1,3], Valerie Awad[1], Locke Ezra-Ros Bonomo[1], David McDermitt[1] and Anthony Bretscher[1,5]

[1]Department of Molecular Biology and Genetics, Weill Institute for Cell and Molecular Biology, Cornell University, Ithaca, NY 14853

[2] Present Address: Unit of Structural Studies of Macromolecular Machines in Cellula, Department of Structural Biology and Chemistry, Institut Pasteur, CNRS UMR3528, Paris, France

[3] Present Address: Blavatnik Institute of Genetics, Harvard Medical School, 25 Shattuck St., Boston MA 02115

[4] These authors contributed equally to this work

[5] Address for correspondence: apb5@cornell.edu (A.B.)

Abstract

Activated Ezrin-Radixin-Moesin (ERM) proteins link the plasma membrane to the actin cytoskeleton to generate domain specific structures, such as microvilli. Among many kinases implicated in ERM activation are the homologs LOK and SLK. CRISPR/Cas9 was used to knockout all ERM proteins or LOK/SLK in human cells. LOK/SLK knockout eliminates all ERM activating phosphorylation. The apical domain of cells lacking LOK/SLK or ERMs is strikingly similar, with loss of microvilli, alterations in junctions, induction of myosin-II containing apical stress-fiber-like structures with enhanced myosin-light-chain (MLC) phosphorylation, and enhanced apical tension. Both knockout lines have elevated active RhoA, revealing that active ERMs are negative regulators of RhoA. Constitutively active ezrin can reverse the phenotypes of either ERMs or LOK/SLK knockouts, showing that the major function of LOK/SLK is to activate ERMs. Thus, LOK/SLK and ERM proteins work as a module to regulate RhoA and contribute to the proper apical morphology of epithelial cells.

Introduction

Essentially all eukaryotic cells are polarized, or have the potential to become polarized. This requires local regulation to define the morphology and composition of each cellular domain. A particularly well studied example is the intestinal epithelial cell with a highly ordered apical domain displaying abundant microvilli and having a protein and lipid composition distinct from the more planar basolateral membrane. While much is known about extrinsic cues that instruct the cell to polarize (Rodriguez-Boulan and Macara, 2014), much less is known about how the morphology of the individual domains is regulated. To address this, we have studied how the apical domain of epithelial cells is regulated to assemble bundles of actin filaments that support the plasma membrane of microvilli, in contrast to the flatter structure of the basolateral membrane.

The structural integrity of apical microvilli requires active ezrin/radixin/moesin (ERM) proteins (Fehon et al., 2010). These proteins exist in a cytoplasmic closed state and an active open conformation where the N-terminal FERM domain binds the plasma membrane and the C-terminal F-actin binding domain binds the underlying actin filaments (Gary and Bretscher, 1995). Activation requires phosphorylation of a conserved threonine, T567 in ezrin (Hayashi et al.,

35 1999; Matsui et al., 1998). In *Drosophila melanogaster*, which has moesin as its single essential
36 ERM protein (Jankovics et al., 2002; Polosello et al., 2002), Slik is the responsible kinase
37 (Hipfner et al., 2004). Among many kinases that have been suggested to activate ERM proteins
38 in vertebrate cells, recent work has focused on the Slik homologues, LOK (lymphocyte-oriented
39 kinase), and the closely related SLK (Ste20-like-kinase), which are appropriately localized to the
40 apical membrane (Pelaseyed and Bretscher, 2018; Cécile Sauvanet et al., 2015). LOK and SLK
41 belong to the germinal center-like kinase (GCK) -V subfamily of kinases (Kuramochi et al.,
42 1997). They consist of a conserved N-terminal kinase domain, a less-conserved intermediate
43 region and a moderately conserved C-terminal domain. The LOK C-terminal domain inhibits the
44 kinase activity of LOK in cells, most likely through a cis-interaction, as well as targeting LOK to
45 the apical membrane (Pelaseyed et al., 2017; Viswanatha et al., 2012). An intricate multi-step
46 mechanism is involved in phosphorylation of ezrin by LOK. In outline, it requires priming of ezrin
47 by PIP_2, then insertion of the C-terminal region of LOK between the ezrin FERM and C-terminal
48 F-actin binding domain, which gives access for the kinase domain to bind a recognition site and
49 ultimately phosphorylate T567 (Pelaseyed et al., 2017). This mechanism, together with the
50 strong preference for a tyrosine two residues upstream of the targeted threonine (Belkina et al.,
51 2009), makes phosphorylation of ERM proteins highly selective. Further, to maintain an apical
52 distribution, ezrin has to undergo phosphorylation/dephosphorylation cycles in which it is locally
53 phosphorylated by LOK and subject to dephosphorylation by delocalized phosphatase
54 Mypt1/PP1. As a result, constitutively active ezrin is unable to maintain apical restriction
55 (Viswanatha et al., 2012).
56
57 The Rho family of small GTP-binding proteins are major regulators of microfilaments
58 (Hall and Nobes, 2000). In early work Speck et al. (Speck et al., 2003) found that defects in fly
59 moesin could be counteracted by antagonizing Rho activity. RhoA is capable of binding to a
60 diverse range of effectors that influence the reorganization of actin into stress fibers and focal
61 adhesions (Hall, 1998). Among these, the effector ROCK modulates microfilament organization
62 and function in at least two distinct ways. First, it activates myosin II by directly phosphorylating
63 the myosin regulatory light chain (Kimura et al., 1996) and inactivating myosin light chain
64 phosphatase (Mypt1/PP1) (Kimura et al., 1996). Second, ROCK stabilizes F-actin by
65 phosphorylating LIM kinase to abrogate its inhibitory activity towards cofilin, an F-actin
66 destabilizing factor (Arber et al., 1998; Maekawa et al., 2017; Yang et al., 1998). The net effect
67 results in an increase of cortical tension that can drive cellular contraction. ERM proteins have

long been suggested to be downstream targets of ROCK, first as direct targets and then as indirect targets through Rho activation of PI-4-P5K (Matsui et al., 1999).

Until recently, the potential relationship between Rho and LOK and SLK had not been studied. A BioID screen for regulators and effectors of RhoA in cultured cells identified SLK (and LOK) as effectors of RhoA (Bagci et al., 2020). RhoA-GTP was shown to bind to the C-terminal domain of SLK, the corresponding domain that negatively regulates the kinase activity and targets LOK to the apical domain. Thus, a direct pathway exists from RhoA-GTP, to LOK/SLK to ERM protein activation.

Uncovering the functions of ERM proteins and LOK and SLK in cultured cells has been hampered by redundancy, and the possibility that they perform essential functions. Here we show that it is possible to generate cultured cells lacking all ERM proteins, and cells lacking both LOK and SLK. This has allowed us to explore the roles of these proteins, both by characterizing cells lacking them, but also by re-introduction of variants. Surprisingly, cells lacking LOK and SLK have a strikingly similar phenotype to cells lacking ERM proteins. Our results establish that LOK and SLK are the major ERM kinases that phosphorylate the conserved threonine. Further, rescue experiments indicate that ERM proteins are the major substrates of LOK and SLK that regulate cell morphology. Moreover, loss of either LOK/SLK or ERM proteins elevates Rho signaling to enhance stress fiber formation in the apical aspect of epithelial cells. We propose that LOK/SLK and ERM proteins function as a module that defines apical morphology of epithelial cells in a process that involves a negative feed-back loop to locally down-regulate Rho activity.

Results

Jeg3 cells lacking ERM proteins or LOK/SLK are viable and lack microvilli

In earlier studies we described human cells modified by CRISPR/Cas9 to lack expression of LOK (Pelaseyed et al., 2017), but so far no cultured cells have been described that genetically lack specific ERM proteins. We set out to determine if cells lacking all ERM proteins, or lacking both LOK and SLK, are viable, and if so, what phenotypes were conferred. Our studies were performed in Jeg3 epithelial cells derived from a human choriocarcinoma as these cells exhibit

102 abundant apical microvilli (Pakkanen et al., 1987). Of the ERM proteins, Jeg3 cells express
103 ezrin and radixin, but not moesin (Figure 1A). We first used CRISPR/Cas9 to isolate cells
104 lacking either ezrin or radixin or SLK (Figure 1A). We then generated pairs of double knockout
105 cells, lacking all detectable ezrin and radixin, or LOK and SLK (Figure 1A). Importantly, moesin
106 was not expressed in the Jeg3 ezrin$^{-/-}$ radixin$^{-/-}$ cells—which can be identified as moesin is
107 expressed in HeLa cells (Figure 1A, lane 1). Thus, the Jeg3 cells lacking all ERM proteins are
108 viable. Likewise, Jeg3 cells lacking both LOK and SLK are viable. However, both ezrin$^{-/-}$ radixin$^{-/-}$
109 and LOK$^{-/-}$ SLK$^{-/-}$ cells grew slower than their wildtype counterparts (Figure S1A).
110
111 As ERM proteins and LOK and SLK have been implicated in the formation of microvilli
112 on these cells, we examined whether single and double knockout cells retained microvilli. To
113 assess the presence of microvilli, we could not use the traditional ERM proteins as markers, so
114 we utilized labelled wheat germ agglutinin (WGA) that binds to plasma membrane glycoproteins
115 and allows for the identification of cell surface structures. In wildtype cells, WGA colocalizes with
116 ezrin in surface microvilli (Figure 1B). Consistent with earlier reports, individual reduction of
117 ezrin or or genetic loss of LOK resulted in a reduction in the number of cells with apical
118 microvilli, whereas loss of radixin or SLK had little phenotype (Figure 1C, Figure S1B). Strikingly
119 ezrin$^{-/-}$ radixin$^{-/-}$ and LOK$^{-/-}$ SLK$^{-/-}$ cells totally lack microvilli, with WGA staining mostly associated
120 with membrane ruffles that form above membrane contact sites (Figure 1B, arrows and 1C).
121 Ezrin is cytosolic in LOK$^{-/-}$ SLK$^{-/-}$ cells, consistent with phosphorylation by LOK/SLK being
122 required to activate it. Stable expression of ezrin in ezrin$^{-/-}$ radixin$^{-/-}$ cells and LOK in LOK$^{-/-}$/SLK$^{-/-}$
123 restored the presence of microvilli to the cell surface. We conclude that both an ERM protein
124 and LOK or SLK are necessary for the presence of apical microvilli. We also examined the
125 localization of the interactor of active ezrin, EBP50 (ERM-binding phosphoprotein of
126 50kD)/NHERF1 (Figure 1D). Whereas EBP50 was present in microvilli in wildtype cells, in both
127 double knockout cell lines EBP50 was cytosolic. Both the WGA and EBP50 staining supports
128 the conclusion that the loss of ERMs or LOK/SLK disrupts the presence of microvilli from the
129 apical surface.
130
131 **LOK/SLK are the major kinases for ERM phosphorylation**
132
133 ERM proteins undergo activation by C-terminal phosphorylation to exhibit their
134 membrane-cytoskeletal linking function (Pearson et al., 2000; Turunen et al., 1994). The identity
135 of the relevant kinase has been controversial (see Discussion), so we assessed the contribution

136 of LOK and SLK to ERM phosphorylation in LOK$^{-/-}$ SLK$^{-/-}$ cells. Using an antibody that detects
137 the relevant epitope on all ERM proteins (phosphorylation of T567 in ezrin, T564 in radixin, and
138 T558 in moesin) we found that LOK$^{-/-}$ SLK$^{-/-}$ cells appeared to be entirely devoid of all ERM
139 phosphorylation (Figure 2A). However, because the pERM antibody produces a small
140 background staining to unphosphorylated ezrin (Pelaseyed et al., 2017), we repeated the
141 experiment employing phos-Tag gels in which phosphorylated ERMs migrate slower than their
142 unphosphorylated counterparts. Again, we were unable to detect any phosphorylated ERM
143 proteins in the absence of LOK and SLK (Figure 2B), so LOK and SLK appear to be the major
144 ERM kinases in Jeg3 cells.
145
146 To explore if this is true in other cells, we also generated LOK$^{-/-}$ SLK$^{-/-}$ knockouts in HeLa
147 cells. While these cells survived clonal isolation and lysate collection, they grew very slowly and
148 could not be maintained. Nevertheless, analysis of cell lysates revealed that in HeLa cells as
149 well, LOK and SLK are the major ERM kinases (Figure 2A). Further, we also tried to knock out
150 LOK and SLK in epithelial Caco-2 cells, which proved inviable past clonal selection indicating
151 the importance of these kinases. Likewise, we tried to isolate HeLa and Caco-2 cells lacking
152 ezrin. Although we nursed the growth of enough cells to demonstrate loss of ezrin, they could
153 not be passaged. These results suggest that ERM proteins are more important for viability in
154 HeLa and Caco-2 cells than in Jeg-3 cells. It was fortuitous that we started with Jeg-3 cells as it
155 has allowed us to use the double knock-outs to explore in more detail the phenotypes conferred
156 by loss of these proteins, or reintroduction of variants.
157
158 In transfection-based experiments, expression of LOK-GFP-Flag was able to both
159 restore ERM phosphorylation and apical microvilli to LOK$^{-/-}$ SLK$^{-/-}$ cells (Figures 1B&C, 2D).
160 LOK contains an N-terminal kinase domain and C-terminal domain responsible for both
161 regulating and localizing the kinase (Pelaseyed et al., 2017). As expected, expression of a
162 K65R kinase-inactive variant of LOK was unable to restore phosphorylation or microvilli (Figure
163 2C,D).
164
165 **Absence of activated ERM proteins induces the formation of apical actin/myosin II**
166 **bundles and alters cell-cell junctions of epithelial cells**
167
168 To explore what additional phenotypes might be associated with loss of ERM proteins
169 and their activating kinases, we examined the structure of cell junctions and the actin

170 distribution in the knockout cells. A characteristic feature of epithelial cells is their ability to form
171 strong cell-to-cell contact sites. Using the tight junction marker ZO-1, we observe a remarkably
172 similar phenotype in ezrin$^{-/-}$ radixin$^{-/-}$ and LOK$^{-/-}$ SLK$^{-/-}$ cells. In both cases, the cells maintain cell-
173 to-cell contacts, but the contact sites are uneven and occasionally have breaks in their ZO-1
174 and reduced junctional actin staining (Figure 3A, magenta arrows). In contrast, wildtype Jeg3
175 cells form uniform and relatively linear contacts along cell junctions co-staining with actin (Figure
176 3A, blue arrows). By determining the ratio between the contour length and shortest distance in
177 ZO-1 staining from a three-cell junction to the next, we quantified the straightness of the tight
178 junctions in various conditions (Figure 3B). This measurement of tortuosity was slightly above
179 1.0 for wildtype cells, reflecting their almost linear nature. For either ezrin$^{-/-}$ or LOK $^{-/-}$ this rose to
180 1.15, and for ezrin$^{-/-}$ radixin$^{-/-}$ and LOK$^{-/-}$/SLK$^{-/-}$ cells to about 1.2, indicating greater
181 distortion/waviness of the interface. As with loss of microvilli, loss of ezrin or LOK is more
182 severe than loss of radixin or SLK, and both double mutants exhibit the most severe phenotype.
183 This tortuosity of the junctions was rescued by expressing ezrin in the ezrin$^{-/-}$ radixin$^{-/-}$ cells and
184 LOK in the LOK$^{-/-}$ SLK$^{-/-}$ cells.
185
186 We also noticed a striking effect on the actin distribution in which significantly more F-
187 actin is seen across the apical domain in the double knockout cells compared to their wild type
188 counterpart. Therefore, we examined the F-actin distribution in the basal and apical regions of
189 the cells. ZO-1 localization is found near the apical region of both wildtype and knockout cells,
190 so we split confocal planes into those containing ZO-1 staining and above (the apical domain),
191 and those below ZO-1 staining (the basolateral domain). Whereas the wildtype cells display
192 actin in microvilli and along the cell junctions, both ezrin$^{-/-}$ radixin$^{-/-}$ and LOK$^{-/-}$/SLK$^{-/-}$ cells were
193 noticeably different with actin bundles extending across the apical domain that correlate with the
194 uneven contour of the tight junctions (Figure 3A). In contrast, there is no apparent difference in
195 the basal actin network between the cells (Figure 3A), which is underscored by the similarity of
196 focal contacts at the basal surfaces (Figure S2A). We quantified this difference by measuring
197 the ratio of the actin intensity at the apical versus the basal side of the cells (Figure 3C). Both
198 KO cells were found to have an increase in the density of actin found exclusively at the apical
199 surface compared to WT cells (Figure 3A and C). The aberrant apical actin bundles are
200 rescued by introduction of ezrin into ezrin$^{-/-}$ radixin$^{-/-}$ and of LOK into LOK$^{-/-}$/SLK$^{-/-}$ cells (Figure 3
201 A-C).
202

203 The apical actin structures seen in ezrin$^{-/-}$ radixin$^{-/-}$ and LOK$^{-/-}$ SLK$^{-/-}$ cells contained
204 bundles, similar in appearance to stress fibers. The expression level of the stress fiber marker α
205 -actinin and focal adhesion marker vinculin were unchanged in the knockout cells (Figure S3).
206 We next explored if these bundles could have contractile properties by staining for non-muscle
207 myosin-IIB (myo-IIB). While striated bundles of myo-IIB and actin were not completely absent in
208 the apical region of wildtype cells, a stronger intensity and more frequent clusters of myo-IIB
209 was observed in ezrin$^{-/-}$ radixin$^{-/-}$ cells (Figure 4A, arrows). This phenotype was also seen and
210 enhanced in LOK$^{-/-}$SLK$^{-/-}$ cells where the entire apical domain appeared covered in myo-IIB
211 puncta and actin filaments. Using deconvolution microscopy, we could see characteristic
212 myosin-II sarcomeric-like striations indicative of a contractile structure (Figure 4B). Together our
213 results show that lack of activated ERMs, either due to loss of the proteins or their activating
214 kinases, selectively redistributes actin into contractile bundles in the apical domain.
215
216 **Enhanced actin assembly in the apical domain is responsible for the junctional defects of**
217 **knockout cells**
218
219 In wildtype cells, apical actin in the microvilli treadmills continuously resulting in turnover
220 in the ~2-10 min time-frame (Loomis et al., 2003; Meenderink et al., 2019). We investigated the
221 possibility that the abnormal actin bundles seen in knockout cells might arise in part from
222 reduced actin turnover in the apical domain. To test this, we treated wildtype cells with the actin
223 stabilizing drug Jasplakinolide to reduce actin turnover. Remarkably, treatment of wildtype cells
224 with 500nM Jasplakinolide for 30 minutes induced both the formation of actin bundles in the
225 apical domain and increased the tortuosity of the tight junctions (Figure 5A and B, lanes 1 and
226 2) in a manner closely resembling the phenotype of ezrin$^{-/-}$ radixin$^{-/-}$ or LOK$^{-/-}$ SLK$^{-/-}$ cells (Figure
227 3A). The addition of Jasplakinolide in all three cell lines further increased the abundance of
228 apical F-actin networks across each cell, correlating with the increased tight junction tortuosity
229 and breaks between neighboring cells (Figure 5A, magenta arrows and C).
230
231 If enhanced actin assembly in the double knockout cells is responsible for the observed
232 tortuosity of the junctions, increasing depolymerization in these cells might rescue this
233 phenotype. Upon treatment of either of the double-knockout cells with the actin-depolymerizing
234 drug Latrunculin B or actin plus-end-capping drug Cytochalasin D, tight junction tortuosity ratios
235 in the knockout cells were restored to levels comparable to wildtype cells (Figure 5A, B and
236 S5A). Interestingly, Latrunculin B treatment of cells did not completely restore the balance of F-

237 actin between the apical and basolateral domains to wild type levels (Figure 5C). Analysis of the
238 apical/basolateral actin distribution after these drug treatments was complicated by the finding
239 that apical actin appears to be more resistant to disassembly by Latrunculin B than its
240 basolateral counterpart (Figure S5B). Nonetheless, in contrast to Jasplakinolide-treated cells,
241 Latrunculin B treatment results in reorganization of actin towards junctions Figure 5A, blue
242 arrows) and relief of junctional defects (Figure 5B). Meanwhile, stabilization by Jasplakinolide
243 redistributes actin away from the junctions and across the cell promoting junctional defects
244 (Figure 5A and B). In summary, our data shows ezrin$^{-/-}$ radixin$^{-/-}$ and LOK$^{-/-}$ SLK$^{-/-}$ cells become
245 more similar to wildtype when treated with Latrunculin B, while wildtype cells become more like
246 the knockout cells when treated with Jasplakinolide. Therefore in the absence of active ERMs,
247 excessive active assembly generates contractile bundles that provide forces perpendicular to
248 junctions.
249
250 To assess how the actin redistribution might affect the mechanics of the apical surface,
251 we utilized Atomic Force Microscopy (AFM) to measure their stiffness. Cells were allowed to
252 grow to a confluent monolayer and then indented to a maximum force of 1nN (Figure 5D inset).
253 The resulting force vs. distance curves were then used to identify the initial AFM probe tip
254 contact point, allowing us to fit to a hertz equation to calculate the Young's modulus (E) stiffness
255 parameter (Huth, Sindt, & Selhuber-Unkel, 2019). Indentations from each condition were then
256 averaged to produce a mean curve for wild type, ezrin$^{-/-}$ radixin$^{-/-}$ and LOK$^{-/-}$ SLK$^{-/-}$ cells (Figure
257 5D). Of the 1,091 total force indentations preformed, both LOK$^{-/-}$ SLK$^{-/-}$ (E = 260±45 kPa
258 Median±) and ezrin$^{-/-}$ radixin$^{-/-}$ (E = 166±52 kPa) cells are significantly stiffer then WT cells (E =
259 117±65 kPa) (Figure 5E). The finding that LOK$^{-/-}$SLK$^{-/-}$ cells are more rigid than ezrin$^{-/-}$ radixin$^{-/-}$
260 cells is consistent with the enhanced levels of stress-fiber-like bundles seen in the apical
261 domain of LOK$^{-/-}$SLK$^{-/-}$ cells described in Figure 4. Together these results indicate that activated
262 ERM proteins suppress the formation of apical actin bundles to affect the mechanical properties
263 of the apical domain.
264
265 **Activated ezrin Rescues both ezrin$^{-/-}$ radixin$^{-/-}$ and LOK$^{-/-}$SLK$^{-/-}$ cells**
266
267 The phenotypic similarity of the ezrin$^{-/-}$ radixin$^{-/-}$ and LOK$^{-/-}$ SLK$^{-/-}$ cells, suggested that
268 essentially all the phenotypes of LOK$^{-/-}$ SLK$^{-/-}$ cells are due to the lack of ERM phosphorylation.
269 If this is the case, introduction of mutationally activated ezrin in either of the double knockout
270 cells should rescue them in a similar manner. We therefore introduced the constitutively active

271 phosphomimetic ezrin-T567D mutant into both ezrin$^{-/-}$ radixin$^{-/-}$ and LOK$^{-/-}$/SLK$^{-/-}$ cells.
272 Remarkably, phosphomimetic ezrin suppressed both equally with restoration of microvilli (Figure
273 6A). The rescue isn't perfect, as constitutively active ezrin is seen both apically and basolaterally
274 because restriction to the apical domain requires ezrin phosphocycling (Viswanatha et al.,
275 2012). Expression of constitutively active phosphomimetic ezrin-T567D is also able to suppress
276 tight junction defects and the excess apical actin bundles seen in knockout cells implying that
277 active ezrin can regulate actin at the cortex (Figure 6B-D). These results suggest that the
278 primary role for LOK and SLK in Jeg3 cells is to phosphorylate ERMs.
279
280 **Phosphorylated ERM proteins regulate myosin-II activity through RhoA Activation**
281
282 We hypothesized that the aberrant apical actin cables and junctional defects seen in the
283 double knockout cells might be a result of either an enhanced level of total non-muscle myosin-
284 II or an increase in the activation of myosin-II. Non-muscle myosin-II is activated by myosin light
285 chain kinase that phosphorylates the myosin light chain 2 (MLC2), and this is counteracted by
286 the phosphatase PP1 utilizing the Mypt1 subunit. Total non-muscle myosin-II expression
287 showed no differences between wild type and LOK$^{-/-}$SLK$^{-/-}$ or ezrin$^{-/-}$ radixin$^{-/-}$ cells (Figure S2B).
288 To explore whether myosin-II activity might be enhanced, the level of endogenous MLC2
289 phosphorylation was found to be very low in wildtype cells and 3-4 fold enhanced in both ezrin$^{-/-}$
290 radixin$^{-/-}$ and LOK$^{-/-}$SLK$^{-/-}$ cells (Figure 7A and B). To increase the level of phosphorylation, we
291 treated cells briefly with calyculin A that inhibits the phosphatase PP1. Treatment of wildtype
292 cells with calyculin A enhanced the level of MLC2 phosphorylation, and greatly enhanced the
293 level seen in both of the knockout lines. These results reveal that activated ERM proteins
294 negatively regulate myosin-II activation.
295
296 To further explore the pathway linking active ERMs to MLC2 phosphorylation, we tested
297 the involvement of Rho-associated kinase (ROCK), which is activated by active RhoA.
298 Treatment of wildtype and double knockout cells with the specific ROCK inhibitor Y-27632
299 equalized phospho-MLC2 levels (Figure 7C), indicating that the enhanced level of phospho-
300 MLC2 seen in knockout cells is upstream of ROCK. We therefore measured the level of
301 endogenous RhoA-GTP by passing total cell lysates over Rhotekin-GST beads and measuring
302 the relative levels of RhoA retained. Both ezrin$^{-/-}$ radixin$^{-/-}$ and LOK$^{-/-}$SLK$^{-/-}$ cells were found to
303 have about a 3-fold higher level of active RhoA than wildtype cells (Figure 7D). In addition to
304 regulating MLC2 phosphorylation, ROCK also regulates actin dynamics through the LIM kinase-

305 cofilin pathway (Arber et al., 1998; Maekawa et al., 2017; Yang et al., 1998), which may explain
306 in part the altered actin dynamics discussed earlier.
307
308 A recent report showed that active RhoA binds directly to the C-terminal domain of SLK
309 and this promotes its dimerization and activation to phosphorylate ERM proteins (Bagci et al.,
310 2020). In earlier work we showed that expression of the C-terminal region of LOK (LOK_310-
311 968-GFP-Flag or LOK-CTD-GFP-Flag) acts as a potent dominant negative to strongly inhibit
312 phosphorylation of ERM proteins (Viswanatha et al., 2012). To explore if this region of LOK
313 binds to RhoA, we expressed LOK-CTD-GFP-Flag either alone or with constitutively active HA-
314 RhoA-L30 and immunoprecipitated with Flag antibodies in WT Jeg3 cells (Figure 7E). RhoA
315 was recovered in the Flag immunoprecipitates, indicating an interaction between the two.
316
317 Collectively these results suggest a model in which the apical domain of epithelial cells is
318 regulated by feedback loops involving ERM (Figure 7F). RhoA activates both the kinases
319 LOK/SLK and ROCK to mediate phosphorylation of ERM proteins and MLC, respectively
320 (Figure 7F). ROCK also negatively regulates PP1, the phosphatase that dephosphorylates both
321 pMLC and pERMs. Phosphorylated ERMs localized exclusively in the apical domain negatively
322 regulate RhoA in a feedback loop.
323
324 **Phosphorylated ERMs negatively regulate myosin contractility**
325
326 If the model presented in Figure 7F is valid, we predicted that a functional difference in
327 contractile force production should exist between wildtype and knockout cells. It is known that
328 cultured cells treated with calyculin A to elevate the level of myosin-II activity will ultimately
329 contract (Ishihara et al., 1989). Therefore, we examined the contraction of spread LOK$^{-/-}$SLK$^{-/-}$
330 and ezrin$^{-/-}$radixin$^{-/-}$ cells compared with wildtype cells in the presence of 10nM Calyculin A over
331 the course of 1 hour. Under this treatment a small fraction of WT cells showed rounding and
332 detachment from the plate. In a dramatic difference, LOK$^{-/-}$SLK$^{-/-}$ and ezrin$^{-/-}$radixin$^{-/-}$ cells
333 showed significant rounding and detachment from neighboring cells in under 30 minutes (Figure
334 8A, Movie S1). We confirmed that the contractility is a result of enhanced myosin-II activity as
335 the Calyculin A induced contraction was prevented by inclusion of the myosin-II inhibitor
336 blebbistatin, which showed no rounding or contraction in any cell type after 1 hour (Figure 8B,
337 Movie S2). These results are in agreement with Figure 7A showing an increased level of MLC
338 phosphorylation in the knockout cells in the presence of calyculin A. However, calyculin A also

339 results in enhanced phosphorylation of ERMs (Viswanatha et al., 2012), so we wished to
340 examine if the contractility difference induced by calyculin A was present in cells where the level
341 of active ezrin was unchanged. To achieve this, we stably expressed the active phosphomimetic
342 ezrin-T567E in double knockout cells. Under these conditions both LOK$^{-/-}$ SLK$^{-/-}$ and ezrin$^{-/-}$
343 radixin$^{-/-}$ cells expressing ezrin-T567E the contraction induced by calyculin A was greatly
344 reduced (Figure 8B, Movie S3). This implies that it is the loss of active ERMs, and not the loss
345 of LOK and SLK independent of ERMs, that regulates the contractility due to enhanced RhoA-
346 GTP.
347
348
349 **Discussion**
350
351 In this study we have investigated the phenotypes conferred by loss of ERM proteins, or
352 their activators, LOK and SLK. In some cells loss of LOK and SLK, or in fact just ezrin in HeLa
353 or Caco-2 cells, are too unhealthy to maintain, indicating that, ERM proteins and their activating
354 kinases can be almost essential. This is consistent with the situation in mice and flies, where
355 loss of ezrin or the single fly ERM protein moesin, is lethal (Jankovics et al., 2002; Saotome et
356 al., 2004). Additionally, the loss of SLK in mouse or the single homolog Slik in the fly are also
357 lethal (Hipfner and Cohen, 2003). Loss of just LOK in the mouse has a more modest phenotype
358 (Belkina et al., 2009), presumably due to partial compensation by SLK. We were fortunate to
359 start with a cell line, Jeg-3, that can tolerate loss of either all ERM proteins, or both LOK and
360 SLK, as this allowed us to study their phenotypes. As far as we are aware, there are the first
361 vertebrate cells isolated genetically lacking either all ERM proteins or the kinases LOK and SLK.
362
363 Previous studies have shown that WT epithelial cells maintain ~50% of their ezrin in the
364 active, phosphorylated state with cycling between active and inactive states occurring on the
365 scale of ~2 minutes (Viswanatha et al., 2012). Proper preservation of this balanced system is
366 critical for maintaining a polarized morphology (Viswanatha et al., 2012) and is consistent with
367 mislocalization, overexpression, and hyper-phosphorylation of ezrin found in types of human
368 cancers (reviewed in Clucas and Valderrama, 2015). The physiologically relevant kinase(s)
369 responsible for ERM phosphorylation has been investigated over decades. Thus, among the
370 many kinases suggested are MST4 (Gloerich et al., 2012; ten Klooster et al., 2009), Rho Kinase
371 (Haas et al., 2007; Matsui et al., 1998), NcK-interacting kinase (Baumgartner et al., 2006) and
372 LOK/SLK (Belkina et al., 2009; Viswanatha et al., 2012). Recent evidence has supported a

373 more unified view suggesting that LOK and SLK may be major vertebrate kinases for ERM
374 phosphorylation (Viswanatha et al., 2012). Our finding that loss of LOK and SLK results in
375 ablation of all detectable ezrin-T567 phosphorylation is consistent with LOK and SLK being the
376 major, if not only, kinases that can phosphoryate the ERM regulatory threonine (T567 in ezrin).
377 This result is in agreement with earlier descriptions that Slik is solely responsible for the
378 activation of fly moesin (Hipfner et al., 2004).
379
380 A remarkable aspect of our results is that cells lacking either ERM proteins or LOK and
381 SLK are phenotypically very similar. Both grow slower, have lost all apical microvilli, have an
382 aberrant level of apical F-actin and myosin, have wavy cell junctions, have a more stiff apical
383 domain, contract abnormally in the presence of the phosphatase calyculin A, and both have
384 elevated levels of Rho-GTP. This raises the question whether the ERM proteins are the sole
385 substrate of LOK/SLK. This potential scenario is consistent with the elaborate coincidence
386 detection and multistep mechanism involved in LOK phosphorylation of ezrin (Pelaseyed et al.,
387 2017). Further, the ability of mutationally active ezrin (ezrin-T567D) to suppress the phenotype
388 of LOK/SLK cells strongly supports the notion that ERM proteins are the major functional
389 substrates, and that LOK/SLK and ERM proteins work together as a functional unit. Using a
390 phospho-proteomics approach in unpublished work, we sought to identify additional LOK/SLK
391 substrates. While we encountered many phosphopeptides whose level was elevated in wild type
392 cells compared with LOK/SLK knockout cells, none had the appropriate LOK/SLK consensus
393 sequence. Although we were not able to identify additional substrates, technical limitations may
394 have obscured them from our analysis. In support of this possibility, the phenotypes of LOK/SLK
395 cells enumerated above were almost always more severe than in the ERM knockout cells. Thus,
396 the possibility that there is another minor substrate, functionally redundant with ERM proteins,
397 cannot be ruled out.
398
399 While we expected to see loss of microvilli in cells lacking ERM proteins, we were
400 surprised to encounter an extensive actin/myosin-II network in the apical domain. This
401 phenotype was also seen in LOK/SLK knockout cells, implying that active ERM proteins can
402 regulate the myosin and actin distribution in the apical domain. RhoA-GTP is known to positively
403 regulate non-muscle myosin-II activity through ROCK as well as F-actin turnover through LIM
404 kinase and cofilin. Both these pathways can promote the depolymerization of actin as non-
405 muscle myosin-II has recently been shown to regulate microvilli actin turnover (Meenderink et
406 al., 2019). Since both actin turnover and myosin contractility are altered in the absence of

407 pERMs, we then considered a possible over-activation of RhoA in the knockout cells. Indeed,
408 the level of RhoA-GTP was significantly elevated in both ERM and LOK/SLK knockout cells.
409 Thus, active ERMs are negative regulators of RhoA (Figure 7F).
410
411 There have been several indications of a connection between ERM protein function and
412 RhoA. First, ROCK was reported as the kinase that phosphorylates ERM proteins, in part
413 because ROCK over expression resulted in formation of microvilli in cos-7 cells and its reported
414 ability to phosphorylate radixin *in vitro* (Matsui et al., 1998; Oshiro et al., 1998). With the finding
415 that Mypt1/PP1 is the phosphatase responsible for dephosphorylating ERM proteins (Fukata et
416 al., 1998), and that Mypt1/PP1 is negatively regulated by ROCK (Velasco et al., 2002), the
417 earlier result can be explained. In a genetic study in the fly, phenotypes resulting from loss of
418 moesin can be rescued by also reducing the level of RhoA (Speck et al., 2003). Recent work
419 has revealed that RhoA-GTP plays a direct role in the dimerization and activation of SLK (Bagci
420 et al., 2020). Together with our finding that phosphorylated ERM proteins act as negative
421 regulators of RhoA-GTP implies local a feedback cycle where RhoA and pERMs regulate each
422 other's activity (Figure 7F).
423
424 RhoA has been well recognized as a regulator of adherens junctions between epithelial
425 cells (reviewed in Hartsock and Nelson, 2008; Marjoram et al., 2014; McCormack et al., 2013).
426 Active Rho is reported to be enriched at cell-cell junctions through the action of various Rho-
427 GEF proteins (Ratheesh et al., 2012; Reyes et al., 2014; Terry et al., 2011). Misregulation of
428 RhoA can affect the mechanical tension between junctions of neighboring epithelial cells (Zihni
429 et al., 2014). Indeed, this is what we observe by knocking out pERMs and upregulating RhoA-
430 GTP. As a consequence of removing pERMs, we find that F-actin bundles are re-distributed
431 away from the junctions and into actomyosin networks across the apical terminal web. The
432 additional pulling forces from the web result in a higher junctional tension (Wakatsuki et al.,
433 2001). This high tension state can be mimicked in wildtype epithelial cells by introducing an
434 actin stabilizing drug like Jasplakinolide. Conversely, the actin can be re-directed back towards
435 junctions by adding actin depolymerizing drug Latrunculin B. A similar phenomenon has also
436 been reported with the disruption of anillin in epithelial cells, in which anillin knockdown cells
437 produce low tensile forces and overexpression produced high tensile forces due to
438 misregulation of medial-apical F-actin (Arnold et al., 2019). Local regulation of polarity-specific
439 proteins like pERMs, anillin and others can, therefore, influence the RhoA-dependent actin
440 turnover at the apical domain and junctions of epithelial cells. As LOK is an effector of active

441 RhoA and is located to the microvilli of epithelial cells, and not the cell-cell junctions, a
442 subpopulation of RhoA must exist in the plasma membrane of microvilli. The activity of this local
443 RhoA population is likely negatively regulated by phosphorylated ERM proteins, presumably
444 through either a Rho-GEF or a Rho-GAP. As there are multiple potential RhoA regulatory
445 molecules, future work will aimed at identifying the factor(s) that allow pERMs to negatively
446 regulate RhoA-GTP locally.

447 A more distant member of the ERM protein family is merlin, the product of the tumor
448 suppressor gene (*NF2*) in which defects result in Neurofibromatosis-II (Sanson et al., 1993;
449 Trofatter et al., 1993). Merlin has an N-terminal FERM domain and a negative regulatory C-
450 terminal. The FERM domain of merlin can bind the C-terminal domain of ERM proteins, and *vice*
451 *versa* (Bretscher et al., 2000). Considerable work suggests that ERM proteins and merlin act
452 antagonistically, especially in the organization of the plasma membrane during endocytosis
453 (Chiasson-Mackenzie et al., 2018; Hebert et al., 2012). It will be interesting to explore if active
454 merlin can regulate RhoA activity, or if merlin-deficient cells that fail to modulate the activity of
455 ERM proteins have a lower level of RhoA-GTP.

456 In summary, we have found that ERM proteins and their activators LOK/SLK function in
457 the same pathway as a unit to build microvilli on the apical surface of epithelial cells and locally
458 reduce the level of RhoA-GTP in a negative feedback cycle. The next challenge will be to
459 understand how this feedback loop is regulated and restricted to the apical domain.

460

461 **Materials and Methods**

462 **Reagents & cDNAs**

463 Ezrin antibodies were either a mouse anti-ezrin antibody (CPCT-ezrin-1 supernatant
464 concentrate obtained from the Developmental Studies Hybridoma) used at 1:1,250 (Western
465 blot) or 1:100 (immunofluorescence) or a previously characterized rabbit polyclonal antibody
466 raised against full-length human ezrin (Bretscher, 1989) and used at 1:1,000 (Western blot) or
467 1:200 (immunofluorescence). Rabbit anti-EBP50 was also a previously characterized antibody
468 (Reczek et al., 1997) and was used at 1:50 (immunofluorescence). Mouse anti-ZO1 (BD
469 Biosciences, Cat #610966) was used at 1:100 (immunofluorescence). Rabbit anti-radixin (Cell
470 Signaling, Cat #C4G7) used at 1:1000 (Western blot) to blot for both radixin (80kDa) and

471 moesin (75kDa). Rabbit anti-pERM (raised against re-combinant phosphopeptide) was used at
472 1:1000 (Western blot). Rabbit anti-LOK used at 1:500 (western blot) and rabbit anti-SLK used at
473 1:100 (Western blot) were purchased from Bethyl Laboratories, Inc. Mouse anti-Flag used at
474 1:5,000 (Western blot) and mouse anti-tubulin used at 1:5,000 (Western blot) were obtained
475 from Sigma-Aldrich. Mouse anti-GFP used at 1:100 (immunofluorescence) was obtained from
476 Santa Cruz Biotechnology, Inc. Rabbit antibodies for anti-myosin-light-chain-2 (Cat #3672) and
477 anti-phospho-myosin-light-chain-2 (raised against phospho-Thr18/Ser19; Cat #3674) were
478 purchased from Cell Signaling and used at 1:500 (Western blot). Monoclonal Mouse anti-RhoA
479 antibody (Cytoskeleton inc. Cat#ARH05) was obtained through the Cytoskeleton inc Rho A
480 activation Assay Biochem Kit and used at 1:500. Rabbit antibody for anti non-muscle-myosin-
481 IIB from (BioLegend, Cat. No. 909902) was used at 1:100 (Western blot and
482 immunofluorescence). Rabbit polyclonal antibodies raised by standard procedures against
483 Vinculin, brush boarder myosin-II and alpha-acitinin purified from chicken gizzard were used at
484 1:2000, 1:200 or 1:200 respectively for supplemental figure 1 western blotting. For actin
485 staining, alexa fluor 488 or 647 phalloidin (Molecular Probes) was used at 1:250. Wheat Germ
486 Agglutinin conjugated to alexa fluor 488 was also purchased from Molecular Probes and used at
487 1:300 to stain cell membranes.

488 Phos-tag was purchased from Wako Chemicals. Jasplakinolide (Cat #11705) and Y-
489 27632 (Cat #100005583-5) were purchased from Cayman Chemicals. DMSO (Cat #D2650),
490 Latrunculin B (Cat #L5288) and Cytochalasin D (Sigma Cat #C8273) were purchased from
491 Sigma-Aldrich. Calyculin A (Cat #BML-El92-0100) was purchased from Enzo Life Sciences and
492 Blebbistatin (Cat #B592500) was purchased from Toronto Research Chemicals.

493 Ezrin point mutants T567E, and T567A were previously generated as described in
494 Viswanatha et al., 2012. Sequences for LOK-GFP-Flag, LOK-CTD-GFP-Flag (or LOK_310-968-
495 GFP-Flag) and LOK-K65R-GFP-Flag were also previously generated in the lab (Pelaseyed et
496 al., 2017; Viswanatha et al., 2012). To generate stable cell lines, ezrin and LOK cDNAs were
497 subcloned into pCDH lentivector (System Biosciences). Puromycin gene in pCDH was then
498 substituted for blasticidin using Gibson assembly. The lentivectors were then transfected with
499 psPAX2 and pCMV-VSVG before virus collection and transduction into Jeg-3 cells. Cells were
500 then grown under blasticidin selection at 5.0 µg/ml for 1-2 weeks prior to immunofluorescent
501 experiments. Stable expression for ezrin was validated using either an ezrin antibody for ezrin
502 constructs or GFP expression for LOK constructs.

503 **Cell culture**

504 Jeg-3, HeLa and Caco-2 cells (ATCC) were maintained in a 5% CO_2 humidified chamber
505 at 37°C. Jeg-3 cells were maintained in MEM with 10% FBS, penicillin/streptomycin and
506 GlutaMax (Thermo Fisher). Cells were cultured on Corning 100mm x 20mm cell culture
507 polystyrene dishes. HeLa and Caco-2 cells were maintained in DMEM with 10% FBS and
508 penicillin/streptomycin. Knockout cell lines were maintained with additional 2.0 µg/ml Puromycin
509 (Sigma) selection. Transient transfections were done using either Lipofectamine 3000
510 (Invitrogen) according to the manufacturer's instructions or polyetheylenimine reagent
511 (PolyPlus) as previously described (Viswanatha et al., 2012).

512 Single guide RNAs (sgRNAs) were designed using CRISPR analysis tools on Benchling
513 and cloned into puromycin-resistant pLenti-CRISPRV2 (AddGene #49535) as described in
514 Sanjana et al., 2014 and Shalem et al., 2014 (Sanjana et al., 2014; Shalem et al., 2014). The
515 following sgRNA sequences were used: 5' - GCAATGTCCGAGTTACCACCA - 3' (ezrin), 5' -
516 AGAAGCAGAACGACTTGAAA - 3' (radixin), 5' - GTAAGACTCACCCAGCATGA - 3' (LOK), 5' -
517 GCAGTACGAACACGTGAAGA - 3' (SLK). Each lentiviral construct was then transfected into
518 293TN cells with psPAX3 and pCMV-VSVG (a gift from Jan Lammerding, WICMB/Cornell,
519 Ithaca, NY) for 48-72 hours before virus collection. Target cells (Jeg3, HeLa or Caco-2) were
520 then transduced with either one or two lentiviruses in order to generate a mixed population of
521 single and double knockout cells. Cells were sorted into single cells and then expanded in
522 puromycin selection before screening by immunofluorescence and Western blotting.

523 Growth curves of Jeg3 cells were preformed by plating cells on low evaporation lid, flat
524 bottom 96 well plates (Corning Cat. #3595). Once plated, cells were seeded at 3,000 cells per
525 well. Plates were then imaged once per hour for 100hrs using a 20X objective using an Incucyte
526 Zoom v2016 (Essen BioSciences) kept in standard cell incubation chamber conditions. Raw
527 data Images were collected and analyzed using Incucyte. Graphs were assembled and
528 exported using Graphpad/Prism (version 8).

529 **Western blotting and immunoprecipitation**

530 Western Blot analysis of cell lysates were done using 6%-12% split SDS-PAGE gels
531 while 6% gel was used for phos-tag experiments. Phos-tag reagent was added at a final
532 concentration of 50uM to a standard Tris-glycine-SDS polyacrylamide gel according to the

533 manufacturer's recommendations. Gels were transferred to a PVDF membrane and blocked
534 with 5% milk in TBS + 0.5% Tween-20. Primary antibodies were incubated with the membrane
535 in 5% bovine serum albumin either for 1 hour at room temperature or overnight at 4°C. Bands
536 were detected with HRP (Thermo Fisher) or infrared fluorescent secondary antibodies
537 (Invitrogen or LI-COR Biosciences). Membranes were imaged using a scanner (Odyssey; LI-
538 COR Biosciences).

539 For detecting myosin-light-chain and phospho-myosin-light-chain, 16% or split 7.5-17.5%
540 SDS-PAGE gels were used and transferred to PVDF membranes with 0.2um pore size was
541 used (Millipour Immuoblion-P^{SQ}). The membrane was then blocked with Immobilon Block-PO
542 phosphoprotein-blocking buffer from EMD-Millipore and incubated with primary antibody
543 solution overnight before developing with chemiluminescent reagents (Radiance Q Plus, Azure
544 Biosystems) on a Bio-Rad ChemiDoc. Relative band intensities were calculated in ImageJ and
545 normalized to a loading control and exported to Graphpad/Prism for statistical analysis.
546 Caylculin A treatments for MLC Blotting were performed by incubating the drug with cells for 10
547 minutes at 37°C prior to lysis. Lysis of cells for MLC blotting was performed with warm (70°C)
548 Laemmli sample buffer, followed by immediate scraping and boiling.

549 To determine an interaction between LOK and constitutively active RhoA-L30, cells were
550 transiently co-transfected with LOK-CTD-GFP-Flag and HA-RhoA-L30 (a kind gift from the
551 Cerione lab, Cornell, Ithaca, NY). After 24 hours, cells were lysed and then solubilized in cold
552 immunoprecipitation buffer (25 mM Tris, pH 7.4, 5% glycerol, 150 mM NaCl, 50 mM NaF, 0.1
553 mM Na3VO4, 10 mM β-glycerol phosphate, 8.7 mg/ml paranitrophenylphosphate, 0.5% Triton
554 X-100, 0.1 μM calyculin A, and protease inhibitor tablet [Roche]) and immunoprecipitated for 2 h
555 using Flag M2 affinity gel (Sigma-Aldrich). Immunoprecipitates were then extensively washed in
556 immunoprecipitation wash buffer (25 mM Tris, pH 7.4, 5% glycerol, 150 mM NaCl, 50 mM NaF,
557 and 0.2% Triton X-100) and then eluted in 200 μg/ml 3×Flag peptide, denatured in Laemmli
558 buffer, resolved by SDS-PAGE, transferred to polyvinylidene difluoride, and developed with
559 HRP western detection.

560 **Active RhoA pull-down**

561 For GTP-RhoA pull down assay the Rho Activation Assay biochem kit (Cytoskeleton inc,
562 Cat# BK036) was used as described in the product manual. In summary, WT Jeg-3 or KO cell
563 lines were plated and grown for 3 days on Corning 100mm x 20mm cell culture polystyrene

564 dishes. An optimum confluency of 70-80% was used as higher confluences can result in partial
565 loss of a monolayer and disruption of apical morphology in Jeg-3 cells. Cells were lysed using
566 the kit lysis buffer and protease inhibitor cocktail then clarified at 10000 x g at 4°C for 1 min. The
567 lysate was then snap frozen in liquid nitrogen as quickly as possible to reduce RhoA-GTP
568 hydrolysis. Frozen lysates were then stored at -80°C. Protein concentrations were measured
569 using the Bradford reagent and absorption at 595nm. Upon thawing aliquots, lysate protein
570 concentration was then normalized to a uniform protein concentration using kit lysis buffer.
571 Equal concentrations of lysate were then passed on 100ug of Rhotekin-RBD beads. The beads
572 were then washed, pelleted and finally boiled with 20ul of Laemmli sample buffer. Positive and
573 negative controls using WT-Jeg 3 lysate incubated with either GTPγs or GDP for 15 minutes
574 prior to passing over the Rhotekin-RBD bead were used to confirm the detectable range of
575 western blot detection, to confirm Rho-A hydrolysis activity and Rhotekin bead binding capacity.
576 Samples were run on a 7.5-17.5% split SDS-PAGE gel and blotted for RhoA; Monoclonal
577 Mouse anti-RhoA antibody (Cytoskeleton inc. Cat#ARH05) was used at 1:500 dilution in TBST
578 overnight.

579 **Time-lapse microscopy, immunofluorescence and image analysis**

580 Cells were treated to a final concentration of 10nM calyculin A diluted into cell media
581 plus 10mM HEPES at the start of time-lapse imaging. Phase contrast images for timecourse
582 movies were taken every 4 minutes for an hour using a 20x objective on a Zeiss AXIO widefield
583 inverted microscope fitted with a 37°C temperature environmental chamber. For blebbistatin
584 experiments, blebbistatin was added to the media to a final concentration of 25uM, 30 minutes
585 prior to addition of calyculin A. For of calyculin A treatment timecourse movies and still frames,
586 imaging was started immediately before addition of calyculin A and time zero was defined as the
587 first captured frame after calyculin A addition.

588 Prior to fixation for immunofluorescence, Jeg3 cells grown on coverslips were washed
589 with PBS and pre-stained with WGA at 1:300 for 30 minutes. For actin turnover experiments in
590 Figure 5A, Jeg3 cells were treated with either DMSO, 500nM Jasplakinolide or 100ng/mL
591 Latrunculin B for 30 min, prior to fixation. Otherwise, for all other immunofluorescent
592 experiments, cells grown on glass coverslips were fixed in 3.7% formalin/PBS for 15 min at
593 room temperature. Cells were then washed with PBS and blocked with immunofluorescence
594 buffer (PBS + 0.5% BSA + 0.5% goat serum + 0.1% Triton X-100) for 10 min. Primary and
595 secondary antibodies were then applied in immunofluorescence buffer containing 2% FBS.

596 Alexa Fluor–conjugated phalloidin, was added to the secondary. The cells were mounted in
597 SlowFade Diamond Antifade (Thermo Fisher) and imaged using a spinning-disk (Yokogawa
598 CSU-X1; Intelligent Imaging Innovations) Leica DMi600B microscope with spherical aberration
599 correction device and a 100/1.46 numerical aperture Leica objective. Images were acquired with
600 a metal-oxide semiconductor device camera (sCMOS) and image slices were assembled using
601 SlideBook 6 software (Intelligent Imaging Innovations). Maximum or summed intensity
602 projections were assembled in SlideBook 6 and exported to Illustrator software (Adobe). For
603 clarity, side projections were vertically expanded using Illustrator. Deconvolution images were
604 captured using an inverted Leica DMi8 wide-field microscope equipped a Leica 506249
605 100X/1.49 oil objective, Leica DFC 9000 GTC camera, with Leica application suit X thunder
606 deconvolution software.

607 The presence or absence of microvilli was scored as described previously (Garbett et
608 al., 2010; Hanono et al., 2006; LaLonde et al., 2010; Pelaseyed et al., 2017; C. Sauvanet et al.,
609 2015). More than 50 cells per replicate were stained using the WGA, ezrin and phalloidin and
610 binned into two categories: microvilli and no microvilli. Microvilli above cell–cell junctions were
611 ignored in the scoring.

612 For calculating tortuosity among tight junctions and relative apical and lateral actin
613 intensities, cells were stained with a ZO-1 antibody and phalloidin and imaged on a spinning-
614 disk microscope as described earlier. To analyze tortuosity, the ZO-1 channel was skeletonized
615 into 1 pixel line widths using ImageJ. Between two consecutive intersection points, a straight-
616 line length was measured and the average of two manually traced line lengths (to account for
617 human variability) along the skeletonized line were also measured. From there, the ratio
618 between the actual line length to the expected line length (straight length) was calculated and
619 exported into Graphpad/Prism for statistical analysis. For comparing actin intensities between
620 apical and lateral regions, Max-Z projections were divided between ZO-1 positive (apical) and
621 ZO-1 negative (lateral) staining. From there, outlines of each cell were traced and measured for
622 their relative mean intensity value in the apical stacks versus the lateral stacks. The ratio
623 between the apical and lateral values were then calculated, plotted and analyzed for statistical
624 significance (Welch's t-test) in GraphPad/Prism.

625 **Atomic Force Microscopy (AFM)**

626 Atomic force microscopy experiments were performed using a MFP-3D-BIOTM Atomic
627 Force Microscope by Asylum Research mounted on an Olympus IX71 inverted microscope that
628 resides on a Herzan AVI 350-S Active Vibration Isolation Table totally enclosed in an air tight
629 BCH-45 Large Acoustic Isolation Hood. Software modules are written in Igor Pro by
630 Wavemetrics. Cells were plated onto WillCo-Dish Glass bottom dish (size 50x7mm. glass
631 30mm. Class #1.5, 0.17mm (Product number GWST-5030; Willco Wells)). Pyramidal shaped
632 Probe TIP (PNP-TR-20) from Asylum Research (804.NW.PNP-TR) were used and calibrated
633 using an in-air calculation of the spring constant. Individual cells within monolayers were
634 selected using phase contrast live imaging with the probe tip location simultaneously illuminated
635 onto the field of view. Probe tips were lowered onto a cell at a velocity of 1000nm/s to a trigger
636 point of 1 nN. Individual cells were force mapped by indenting 100 times over a square 20μm x
637 20μm area. Simultaneous force indentation and membrane retraction measurements were
638 made by first incubating probe tips with 3.0mg/ml of concanavalin A in PBS buffer for 1.5 hours
639 at room temperature. Deflection and z-probe position data was exported into matlab then
640 analyzed using the open access software from Huth and colleagues (Huth et al., 2019) modified
641 for a pyramidal shape probe tip. Force indentation traces were filtered for single force peaks
642 then chi-value goodness fit to the Hertz model. Youngs modulus statistical analysis and
643 graphing of AFM data was performed in Graphpad/Prism.
644

645 **Acknowledgements**

646 We thank the University of Vermont College of Medicine Microscopy Imaging Center,
647 specifically D. Taatjes and N. Bouffard for their help using the Asylum Research MFP-3 D BIO
648 atomic force microscope. The microscope was purchased with support from NIH award number
649 S10RR025498 from the National Center for Research Resources (to DT). We thank Alan Howe
650 (University of Vermont) for his suggestions on Myosin Light Chain detection and Steven Huth
651 (Christian-Albrechts University of Keil) for his help implementing AFM Hertz fit analysis to our
652 data. We thank Jan Lammerding (Cornell University) for his generosity with reagents and use of
653 equipment and Adam Martin (MIT) for his helpful discussions and reviewing the manuscript. We
654 appreciate the effort by Shannon Marshall and Marcus Smolka (Cornell University) with
655 attempts to identify additional LOK phosphorylation targets. This work was supported by NIH
656 Grants RO1 GM036552 and R35 GM131751 to A.B.

Figures

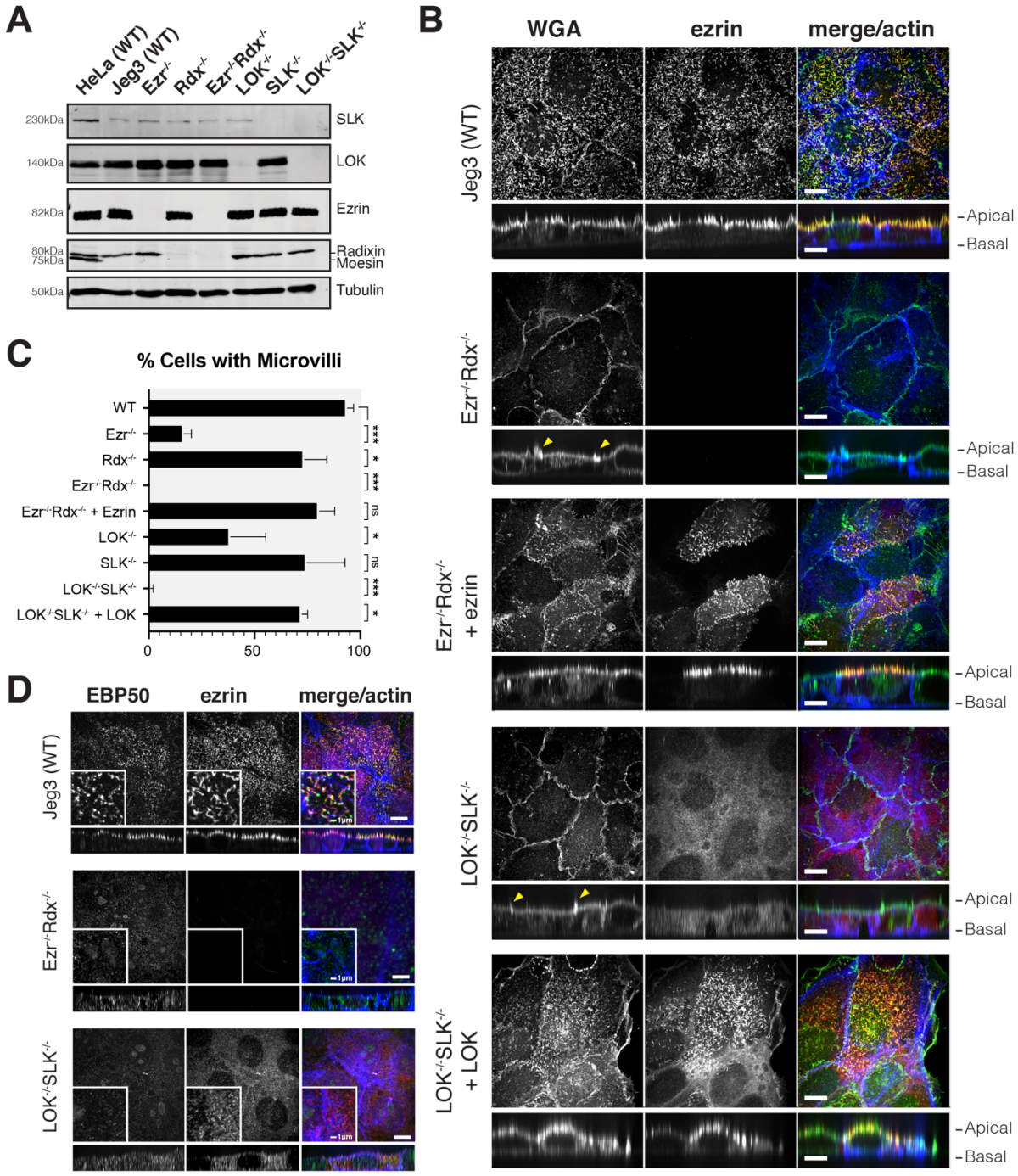
A
HeLa (WT)
Jeg3 (WT)
Ezr-/-
Rdx-/-
Ezr-/-Rdx-/-
LOK-/-
SLK-/-
LOK-/-SLK-/-
230kDa
SLK
140kDa
LOK
82kDa
Ezrin
80kDa
75kDa
Radixin
Moesin
50kDa
Tubulin
B
WGA
ezrin
merge/actin
Jeg3 (WT)
Ezr-/-Rdx-/-
Ezr-/-Rdx-/- + ezrin
LOK-/-SLK-/-
LOK-/-SLK-/- + LOK
Apical
Basal
C
% Cells with Microvilli
WT
Ezr-/-
Rdx-/-
Ezr-/-Rdx-/-
Ezr-/-Rdx-/- + Ezrin
LOK-/-
SLK-/-
LOK-/-SLK-/-
LOK-/-SLK-/- + LOK
***
*
***
ns
*
ns
***
*
0
50
100
D
EBP50
ezrin
merge/actin
Jeg3 (WT)
Ezr-/-Rdx-/-
LOK-/-SLK-/-
1µm

Figure 1: Jeg3 cells lacking ERM proteins or LOK/SLK are viable and lack microvilli. (A) Protein expression using indicated antibodies in western blots of ERM proteins and LOK and SLK in Jeg3 CRISPR cell lysates. HeLa cell lysate was used as a control for expression of moesin, which is not present in Jeg3. Tubulin expression was used as a loading control. (B) Jeg3 cell lines lacking ERM expression or LOK and SLK expression were stained with Wheat-Germ-Agglutinin (WGA), ezrin and actin. Yellow arrows indicate strong membrane ruffles. (C) Percentage of cells expressing microvilli. Bars represents mean±SEM, N=3. Non-significant (ns) p-values are as follows: Ezr $^{-/-}$ Rdx $^{-/-}$ + ezrin = 0.0770 ; LOK $^{-/-}$ SLK $^{-/-}$ + LOK = 0.2079. (D) Staining of cells with EBP50, ezrin and actin in the indicated cells. Scale bars, 10μm unless otherwise noted. Vertical sections were expanded three-fold for clarity. P-values were calculated with Welch's t-test (* $p \leq 0.05$, ** $p \leq 0.01$, *** $p \leq 0.001$).

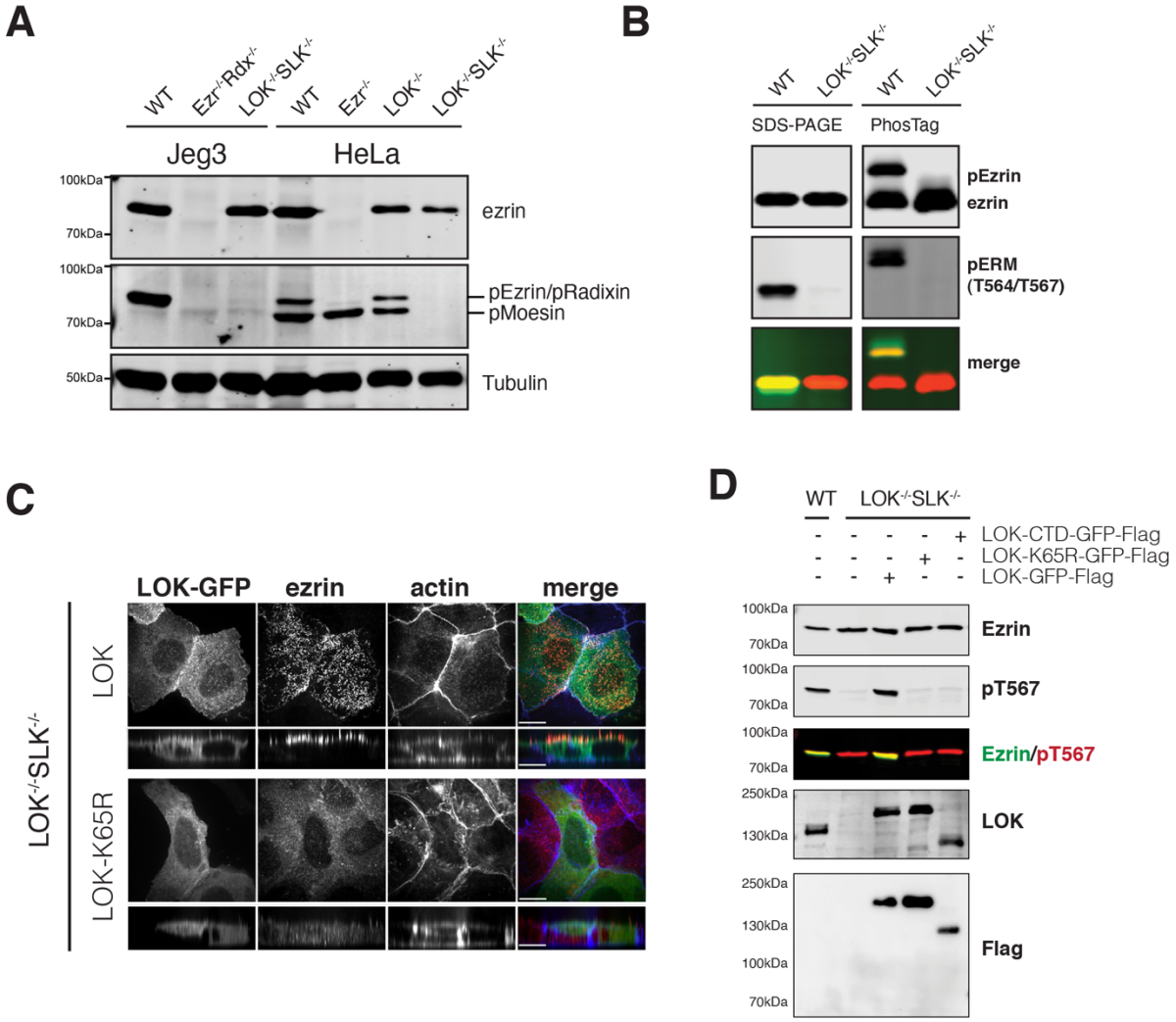
A
WT
Ezr-/-Rdx-/-
LOK-/-SLK-/-
WT
Ezr-/-
LOK-/-
LOK-/-SLK-/-
Jeg3
HeLa
100kDa
70kDa
ezrin
100kDa
70kDa
pEzrin/pRadixin
pMoesin
50kDa
Tubulin
B
WT
LOK-/-SLK-/-
WT
LOK-/-SLK-/-
SDS-PAGE
PhosTag
pEzrin
ezrin
pERM
(T564/T567)
merge
C
LOK-GFP
ezrin
actin
merge
LOK-/-SLK-/-
LOK
LOK-K65R
D
WT
LOK-/-SLK-/-
- - - - + LOK-CTD-GFP-Flag
- - - + - LOK-K65R-GFP-Flag
- - + - - LOK-GFP-Flag
100kDa
70kDa
Ezrin
100kDa
70kDa
pT567
100kDa
70kDa
Ezrin/pT567
250kDa
130kDa
LOK
250kDa
130kDa
100kDa
70kDa
Flag

Figure 2: LOK/SLK are the major ERM kinases. (A) Ezrin and phospho-ERM levels in Jeg3 or HeLa knockout cells. Tubulin is used as a loading control. (B) Extracts of wildtype or $LOK^{-/-}SLK^{-/-}$ cells were resolved by either 6% SDS-PAGE gel or 6% Mn-Phos-Tag SDS-PAGE gel and blotted for ezrin and phosphoERM. Approximately half of endogenous ezrin is phosphorylated in wildtype cells as seen by the shift in band size. No phospho-shift is detected in $LOK^{-/-}SLK^{-/-}$ cells. (C) $LOK^{-/-}SLK^{-/-}$ cells transfected with either LOK-GFP-flag or K65R-LOK-GFP-flag and then co-stained with ezrin and actin. K65R-LOK is unable to rescue apical ezrin localization. (D) Extracts of cells transfected with wildtype LOK or LOK mutants were collected and blotted for endogenous ezrin or phosphoERM. Lysates were also blotted for flag or LOK to check expression of the constructs relative to wildtype LOK. Scale bars 10μm.

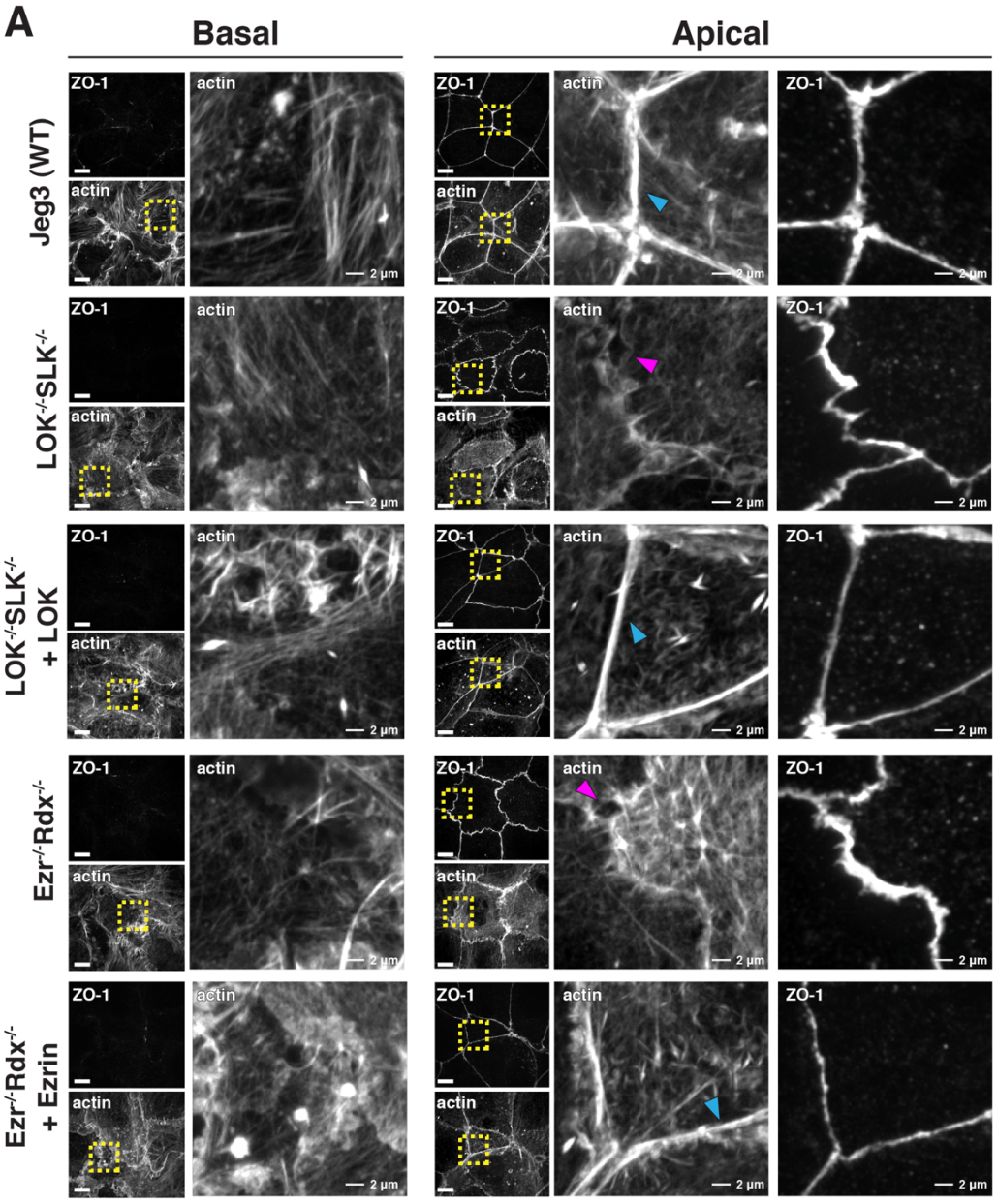
A
Basal
Apical
Jeg3 (WT)
LOK-/-SLK-/-
LOK-/-SLK-/- + LOK
Ezr-/-Rdx-/-
Ezr-/-Rdx-/- + Ezrin
ZO-1
actin
2 µm

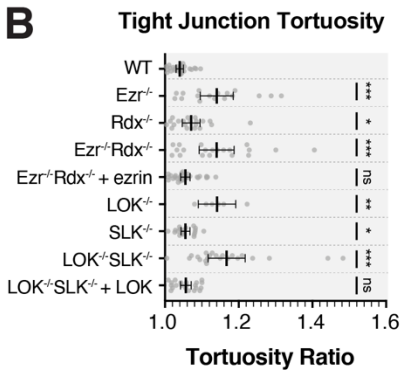
B
Tight Junction Tortuosity
WT
Ezr-/-
Rdx-/-
Ezr-/-Rdx-/-
Ezr-/-Rdx-/- + ezrin
LOK-/-
SLK-/-
LOK-/-SLK-/-
LOK-/-SLK-/- + LOK
***
*
***
ns
**
*
***
ns
1.0
1.2
1.4
1.6
Tortuosity Ratio

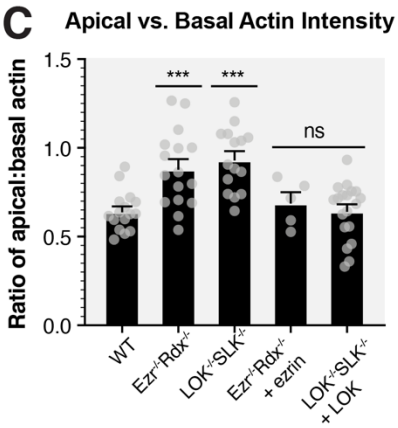
C
Apical vs. Basal Actin Intensity
Ratio of apical:basal actin
1.5
1.0
0.5
0.0
***
***
ns
WT
Ezr-/-Rdx-/-
LOK-/-SLK-/-
Ezr-/-Rdx-/- + ezrin
LOK-/-SLK-/- + LOK

Figure 3: Absence of activated ERM proteins induces the formation of apical actin bundles, alters cell-cell junctions, and compromises the apical rigidity of epithelial cells. (A) Comparison of ZO-1 and actin between basolateral and apical confocal slices. Apical Z-slices were determined by the presence of ZO-1. Blue arrows indicate actin present at cell junctions. Magenta arrows point to actin breaks between neighboring cells. Scale 10μm unless otherwise noted. (B) Quantification of tight junction tortuosity using ZO-1 staining. Each point represents the tortuosity from one tight junction intersection to the next intersection. Center lines respresent mean±SEM. Non-significant (ns) p-values are as follows: Ezr $^{-/-}$ Rdx $^{-/-}$ + ezrin = 0.0578 ; LOK $^{-/-}$ SLK $^{-/-}$ + LOK = 0.0573. (C) The ratios of relative mean actin intensity values per cell between apical and basolateral cross-sections. Bars represent mean±SEM. Non-significant p-values are as follows: Ezr $^{-/-}$ Rdx $^{-/-}$ + ezrin = 0.4188 ; LOK $^{-/-}$ SLK $^{-/-}$ + LOK = 0.9555. P-values were calculated with Welch's t-test (* $p \leq 0.05$, ** $p \leq 0.01$, *** $p \leq 0.001$).

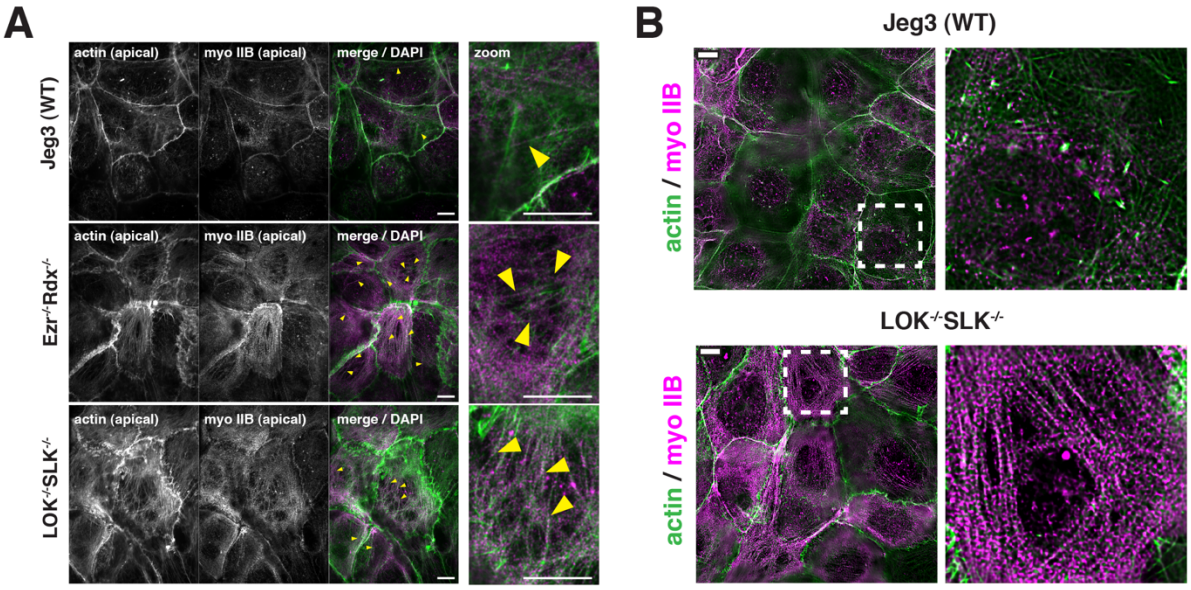
A
actin (apical)
myo IIB (apical)
merge / DAPI
zoom
Jeg3 (WT)
Ezr-/-Rdx-/-
LOK-/-SLK-/-
B
Jeg3 (WT)
actin / myo IIB
LOK-/-SLK-/-

Figure 4: A dense actomyosin network forms at the apical surface of ERM and LOK/SLK knockout cells (A) Maximum projection of immunofluorescence images of the apical confocal Z-slices (2.8μm or 10 confocal slices) indicating actin and non-muscle myosin IIB localization. Areas with contractile fibers are indicated by yellow arrows. (B) Similar apical max projection from deconvolution imaging of the same samples as in (A) showing numerous non-muscle myosin puncta along the apical actin bundles in LOK/SLK knockout cells. Scale bars 10μm.

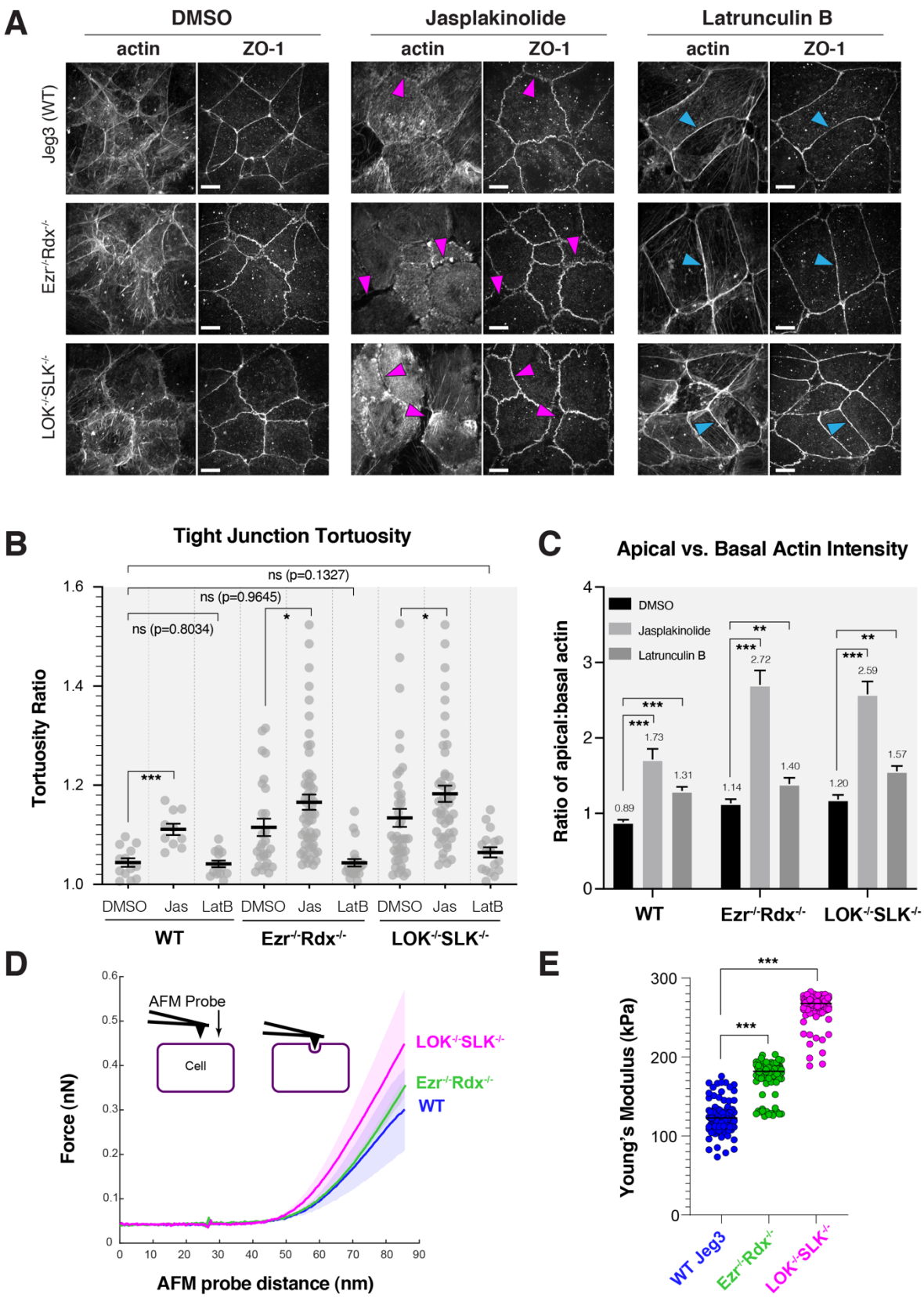
A
DMSO
Jasplakinolide
Latrunculin B
actin
ZO-1
Jeg3 (WT)
Ezr-/-Rdx-/-
LOK-/-SLK-/-
B
Tight Junction Tortuosity
ns (p=0.1327)
ns (p=0.9645)
ns (p=0.8034)
Tortuosity Ratio
DMSO
Jas
LatB
WT
Ezr-/-Rdx-/-
LOK-/-SLK-/-
C
Apical vs. Basal Actin Intensity
Ratio of apical:basal actin
DMSO
Jasplakinolide
Latrunculin B
0.89
1.73
1.31
1.14
2.72
1.40
1.20
2.59
1.57
D
AFM Probe
Cell
Force (nN)
AFM probe distance (nm)
LOK-/-SLK-/-
Ezr-/-Rdx-/-
WT
E
Young's Modulus (kPa)
WT Jeg3
Ezr-/-Rdx-/-
LOK-/-SLK-/-

Figure 5: Increased actin polymerization in ERM or LOK/SLK knockout cells leads to junctional defects and mechanical stiffening of the cell. (A) Jeg3 cells treated with DMSO, 500nM Jaspakinolide or 100ng/mL Latrunculin B for 30 min before immunostaining with ZO-1 and actin. Magenta arrows point to actin gaps at junctions while blue arrows represent actin present at cell junctions. Scale bars, 10 µm. (B) Quantification of tortuosity between tight junction markers as described in Figure 3. Jasplakinolide treatment increases tortuosity values, while Latrunculin B rescues tortuosity to wildtype levels. N ≥ 10 cells per condition. Lines represent mean±SEM. P-values were calculated with Welch's t-test (* $p \leq 0.05$, ** $p \leq 0.01$, *** $p \leq 0.001$). (C) Comparison of actin levels between apical and basolateral regions after treatment with drugs as visualized in panel A. N ≥ 21 cells per condition. Bars show mean±SEM. (D) Averaged force indentation curves for WT Jeg3 (blue), ezrin$^{-/-}$radixin$^{-/-}$ (green) and LOK$^{-/-}$ SLK$^{-/-}$ (magenta); semi-transparent area around each line represents the SEM of the data. A steeper curve indicates a stiffer cell. (E) Young's modulus stiffness parameters; black line indicates each condition's mean value (WT N=356, ezrin$^{-/-}$radixin$^{-/-}$ N=304, LOK$^{-/-}$ SLK$^{-/-}$ N=431). Both KO conditions were significantly stiffer than WT cells (*** $p=<0.0001$, K/S Test).

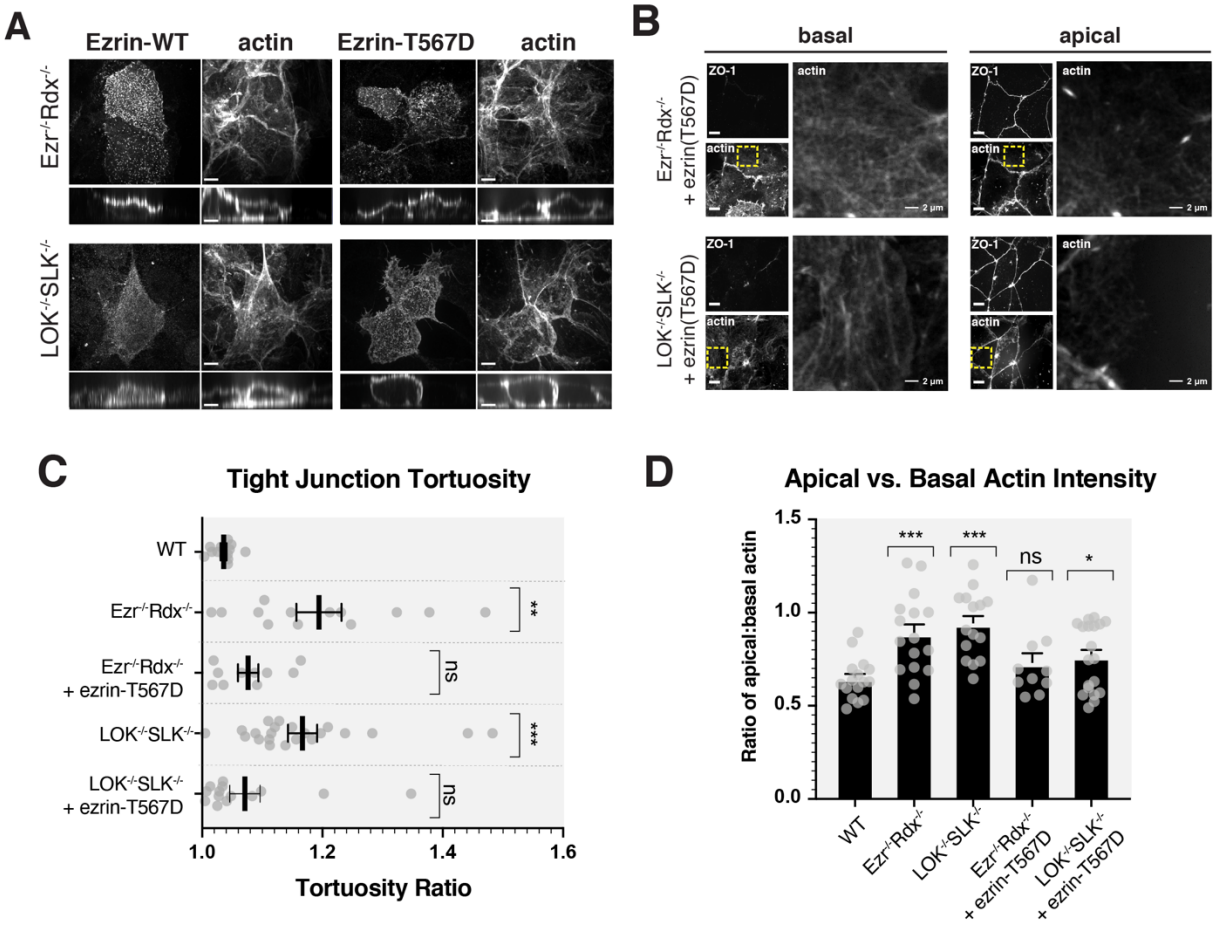
A
Ezrin-WT
actin
Ezrin-T567D
actin
Ezr-/-Rdx-/-
LOK-/-SLK-/-
B
basal
apical
ZO-1
actin
Ezr-/-Rdx-/- + ezrin(T567D)
LOK-/-SLK-/- + ezrin(T567D)
2 µm
C
Tight Junction Tortuosity
WT
Ezr-/-Rdx-/-
Ezr-/-Rdx-/- + ezrin-T567D
LOK-/-SLK-/-
LOK-/-SLK-/- + ezrin-T567D
**
ns
***
ns
1.0
1.2
1.4
1.6
Tortuosity Ratio
D
Apical vs. Basal Actin Intensity
Ratio of apical:basal actin
1.5
1.0
0.5
0.0
***
***
ns
*
WT
Ezr-/-Rdx-/-
LOK-/-SLK-/-
Ezr-/-Rdx-/- + ezrin-T567D
LOK-/-SLK-/- + ezrin-T567D

Figure 6: Constitutively active ezrin rescues apical actin distribution in knockout cells. (A) Jeg3 knockout cells expressing wildtype ezrin or T567 phosphomimetic were stained for ezrin and actin. Maximum intensity projections and vertical cross-sections are shown. (B) Comparison of ZO-1 and actin between basolateral and apical confocal slices between Jeg-3 knockout cells expressing phosphomimetic ezrin-T567D. Apical Z-slices were determined by the presence of ZO-1. Yellow boxes indicate the region of the image that was expanded on the right. (C) Quantification of tight junction tortuosity using ZO-1 staining. N ≥ 10 cells per condition. Center lines show mean±SEM. Non-significant (ns) p-values are as follows: Ezr $^{-/-}$ Rdx $^{-/-}$ + ezrin-T567D = 0.0623; LOK $^{-/-}$ SLK $^{-/-}$ + ezrin-T567D = 0.2445 (D) The ratios of relative mean actin intensity values per cell between apical and basolateral cross-sections. N ≥ 21 cells per condition. Non-significant p-value for Ezr $^{-/-}$ Rdx $^{-/-}$ + ezrin-T567D = 0.4188. Bars show mean±SEM. P-values were calculated against wildtype with Welch's t-test (* p≤0.05, ** p≤0.01, *** p≤0.001). Scale bars, 10μm; unless otherwise noted.

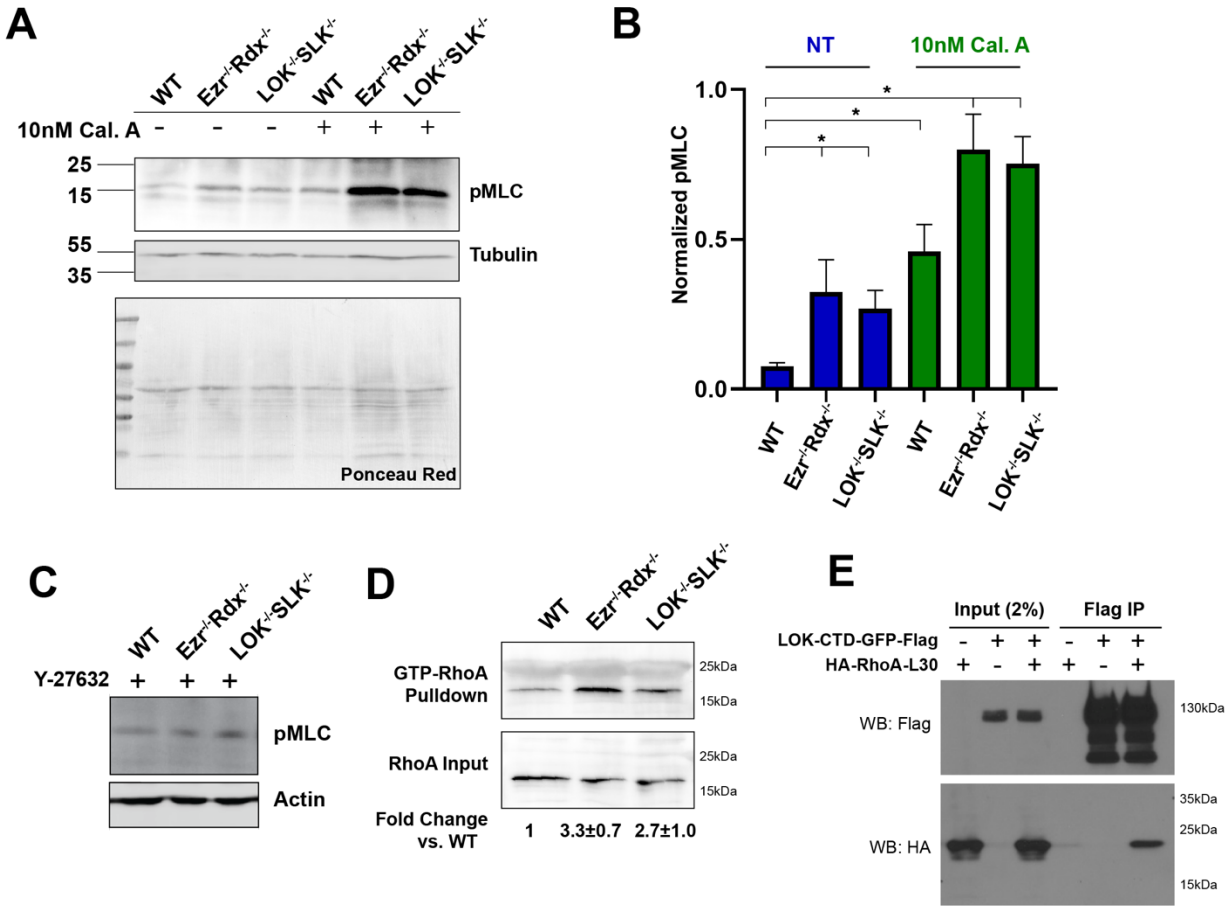
A
WT
Ezr-/-Rdx-/-
LOK-/-SLK-/-
WT
Ezr-/-Rdx-/-
LOK-/-SLK-/-
10nM Cal. A
- - - + + +
25
15
pMLC
55
35
Tubulin
Ponceau Red
B
NT
10nM Cal. A
Normalized pMLC
1.0
0.5
0.0
*
*
*
WT
Ezr-/-Rdx-/-
LOK-/-SLK-/-
WT
Ezr-/-Rdx-/-
LOK-/-SLK-/-
C
WT
Ezr-/-Rdx-/-
LOK-/-SLK-/-
Y-27632 + + +
pMLC
Actin
D
WT
Ezr-/-Rdx-/-
LOK-/-SLK-/-
GTP-RhoA Pulldown
25kDa
15kDa
RhoA Input
25kDa
15kDa
Fold Change vs. WT
1 3.3±0.7 2.7±1.0
E
Input (2%)
Flag IP
LOK-CTD-GFP-Flag - + + - + +
HA-RhoA-L30 + - + + - +
WB: Flag
130kDa
WB: HA
35kDa
25kDa
15kDa
F
RhoA-GTP
LOK/SLK
ROCK
LIMK
Cofilin
F-actin
pERM
MLC
PP1
Mypt1

Figure 7: Phosphorylated ERMs negatively regulate myosin activation through RhoA. (A) Phospho-myosin light chain (pMLC) (T18/S19) western blot with tubulin and total protein staining to indicate equal loading. (B) Quantification of pMLC staining normalized to loading control (bars show mean±SEM; control:N = 4; 10 min of 10nM CalA: N = 3). (C) Western blot of pMLC with actin loading control in Jeg3 cells first treated with ROCK inhibitor Y-27632 showing reversal of the pMLC hyperphosphorylation phenotype in KO cells. (D) Representative Western blot of active RhoA-GTP pull down results. Upper row: Rho-A blot of the Rhotekin beads following pulldown, Lower row: blot of Rho-A of 4% of input lysate. Normalized fold change of the RhoA pull down band intensity compared to WT (mean±SEM; N = 5). (E) LOK-CTD-GFP-Flag pulldown of cells expressing constitutively active RhoA (RhoA-L30) indicating that C-term LOK binds active RhoA. (F) Model of Rho A signaling negatively regulated by phospho-ERMs (dotted blue line).

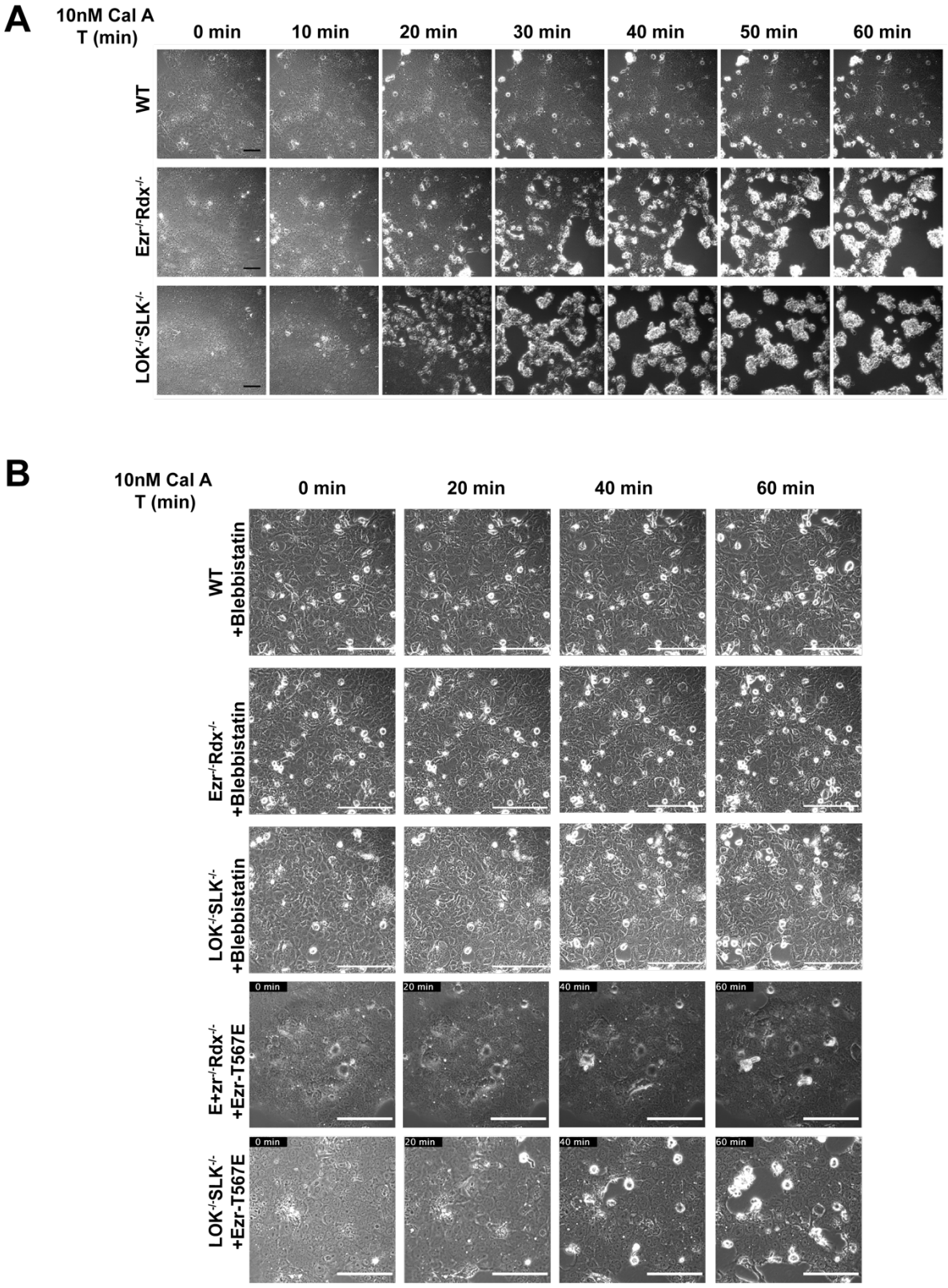
A
10nM Cal A
T (min)
0 min
10 min
20 min
30 min
40 min
50 min
60 min
WT
Ezr-/-Rdx-/-
LOK-/-SLK-/-
B
10nM Cal A
T (min)
0 min
20 min
40 min
60 min
WT +Blebbistatin
Ezr-/-Rdx-/- +Blebbistatin
LOK-/-SLK-/- +Blebbistatin
E+zr-/-Rdx-/- +Ezr-T567E
LOK-/-SLK-/- +Ezr-T567E

Figure 8: Phosphorylated ERMs negatively regulate myosin contractility. (A) Representative phase contrast still images from movies (S1) showing the effect of 10nM calyculin A on WT or KO Cells. (B) Same as (A) except for 30 min treatment with 25uM blebbistatin (Movie S2), or transfection to express phosphomimetic ezrin-T567E (Movie S3), prior to calyculin A treatment. Scales 100μm.

CITATIONS

Arber S, Barbayannis FA, Hanser H, Schnelder C, Stanyon CA, Bernards O, Caroni P. 1998. Regulation of actin dynamics through phosphorylation of cofilin by LIM- kinase. *Nature* **393**:805–809. doi:10.1038/31729

Arnold TR, Shawky JH, Stephenson RE, Dinshaw KM, Higashi T, Huq F, Davidson LA, Miller AL. 2019. Anillin regulates epithelial cell mechanics by structuring the medial-apical actomyosin network. *Elife* **8**:39065. doi:10.7554/eLife.39065

Bagci H, Sriskandarajah N, Robert A, Boulais J, Elkholi IE, Tran V, Lin Z-YY, Thibault M-PP, Dubé N, Faubert D, Hipfner DR, Gingras A-CC, Côté J-FF. 2020. Mapping the proximity interaction network of the Rho-family GTPases reveals signalling pathways and regulatory mechanisms. *Nat Cell Biol* **22**:120–134. doi:10.1038/s41556-019-0438-7

Baumgartner M, Sillman AL, Blackwood EM, Srivastava J, Madson N, Schilling JW, Wright JH, Barber DL. 2006. The Nck-interacting kinase phosphorylates ERM proteins for formation of lamellipodium by growth factors. *Proc Natl Acad Sci U S A* **103**:13391–13396. doi:10.1073/pnas.0605950103

Belkina N V., Liu Y, Hao J-JJJ, Karasuyama H, Shaw S. 2009. LOK is a major ERM kinase in resting lymphocytes and regulates cytoskeletal rearrangement through ERM phosphorylation. *Proc Natl Acad Sci U S A* **106**:4707–4712. doi:10.1073/pnas.0805963106

Bretscher A. 1989. Rapid phosphorylation and reorganization of ezrin and spectrin accompany morphological changes induced in A-431 cells by epidermal growth factor. *J Cell Biol* **108**:921–930. doi:10.1083/jcb.108.3.921

Bretscher A, Chambers D, Nguyen R, Reczek D. 2000. ERM-Merlin and EBP50 Protein Families in Plasma Membrane Organization and Function. *Annu Rev Cell Dev Biol* **16**:113–143. doi:10.1146/annurev.cellbio.16.1.113

Chiasson-Mackenzie C, Morris ZS, Liu CH, Bradford WB, Koorman T, McClatchey AI. 2018. Merlin/ERM proteins regulate growth factor-induced macropinocytosis and receptor recycling by organizing the plasma membrane:Cytoskeleton interface. *Genes Dev* **32**:1201–1214. doi:10.1101/gad.317354.118

Clucas J, Valderrama F. 2015. ERM proteins in cancer progression. *J Cell Sci* **128**:1253–1253. doi:10.1242/jcs.170027

Fehon RG, McClatchey AI, Bretscher A. 2010. Organizing the cell cortex: The role of ERM proteins. *Nat Rev Mol Cell Biol* **11**:276–287. doi:10.1038/nrm2866

Fukata Y, Kimura K, Oshiro N, Saya H, Matsuura Y, Kaibuchi K. 1998. Association of the myosin-binding subunit of myosin phosphatase and moesin: Dual regulation of moesin phosphorylation by Rho-associated kinase and myosin phosphatase. *J Cell Biol* **141**:409–418. doi:10.1083/jcb.141.2.409

Garbett D, LaLonde DP, Bretscher A. 2010. The scaffolding protein EBP50 regulates microvillar assembly in a phosphorylation-dependent manner. *J Cell Biol* **191**:397–413. doi:10.1083/jcb.201004115

Gary R, Bretscher A. 1995. Ezrin self-association involves binding of an N-terminal domain to a normally masked C-terminal domain that includes the F-actin binding site. *Mol Biol Cell* **6**:1061–75. doi:10.1091/mbc.E12-02-0152

Gloerich M, Ten Klooster JP, Vliem MJ, Koorman T, Zwartkruis FJ, Clevers H, Bos JL. 2012. Rap2A links intestinal cell polarity to brush border formation. *Nat Cell Biol* **14**:793–801. doi:10.1038/ncb2537

Haas MA, Vickers JC, Dickson TC. 2007. Rho kinase activates ezrin-radixin-moesin (ERM) proteins and mediates their function in cortical neuron growth, morphology and motility in vitro. *J Neurosci Res* **85**:34–46. doi:10.1002/jnr.21102

Hall A. 1998. Rho GTpases and the actin cytoskeleton. *Science (80-)* **279**:509–514. doi:10.1126/science.279.5350.509
Hall A, Nobes CD. 2000. Rho GTPases: Molecular switches that control the organization and dynamics of the actin cytoskeleton. *Philos Trans R Soc B Biol Sci* **355**:965–970. doi:10.1098/rstb.2000.0632
Hanono A, Garbett D, Reczek D, Chambers DN, Bretscher A. 2006. EPI64 regulates microvillar subdomains and structure. *J Cell Biol* **175**:803–813. doi:10.1083/jcb.200604046
Hartsock A, Nelson WJ. 2008. Adherens and tight junctions: Structure, function and connections to the actin cytoskeleton. *Biochim Biophys Acta - Biomembr*. doi:10.1016/j.bbamem.2007.07.012
Hayashi K, Yonemura S, Matsui T, Tsukita S. 1999. Immunofluorescence detection of ezrin/radixin/moesin (ERM) proteins with their carboxyl-terminal threonine phosphorylated in cultured cells and tissues. *J Cell Sci* **112**:1149–1158.
Hebert AM, DuBoff B, Casaletto JB, Gladden AB, McClatchey AI. 2012. Merlin/ERM proteins establish cortical asymmetry and centrosome position. *Genes Dev* **26**:2709–2723. doi:10.1101/gad.194027.112
Hipfner DR, Cohen SM. 2003. The Drosophila sterile-20 kinase slik controls cell proliferation and apoptosis during imaginal disc development. *PLoS Biol* **1**:244–256. doi:10.1371/journal.pbio.0000035
Hipfner DR, Keller N, Cohen SM. 2004. Slik Sterile-20 kinase regulates Moesin activity to promote epithelial integrity during tissue growth. *Genes Dev* **18**:2243–2248. doi:10.1101/gad.303304
Ishihara H, Martin BL, Brautigan DL, Karaki H, Ozaki H, Kato Y, Fusetani N, Watabe S, Hashimoto K, Uemura D, Hartshorne DJ. 1989. Calyculin A and okadaic acid: Inhibitors of protein phosphatase activity. *Biochem Biophys Res Commun* **159**:871–877. doi:10.1016/0006-291X(89)92189-X
Jankovics F, Sinka R, Lukácsovich T, Erdélyi M. 2002. MOESIN crosslinks actin and cell membrane in Drosophila oocytes and is required for OSKAR anchoring. *Curr Biol* **12**:2060–2065. doi:10.1016/S0960-9822(02)01256-3
Kimura K, Ito M, Amano M, Chihara K, Fukata Y, Nakafuku M, Yamamori B, Feng J, Nakano T, Okawa K, Iwamatsu A, Kaibuchi K. 1996. Phosphorylation and activation of myosin by Rho-associated kinase (Rho- kinase). *J Biol Chem* **271**:20246–20249. doi:10.1074/jbc.271.34.20246
Kuramochi S, Moriguchi T, Kuida K, Endo J, Semba K, Nishida E, Karasuyama H. 1997. LOK is a novel mouse STE20-like protein kinase that is expressed predominantly in lymphocytes. *J Biol Chem* **272**:22679–22684. doi:10.1074/jbc.272.36.22679
LaLonde DP, Garbett D, Bretscher A. 2010. A regulated complex of the scaffolding proteins PDZK1 and EBP50 with ezrin contribute to microvillar organization. *Mol Biol Cell* **21**:1519–29. doi:10.1091/mbc.E10-01-0008
Loomis PA, Zheng L, Sekerková G, Changyaleket B, Mugnaini E, Bartles JR. 2003. Espin cross-links cause the elongation of microvillus-type parallel actin bundles in vivo. *J Cell Biol* **163**:1045–1055. doi:10.1083/jcb.200309093
Maekawa H, Neuner A, Rüthnick D, Schiebel E, Pereira G, Kaneko Y. 2017. Polo-like kinase Cdc5 regulates Spc72 recruitment to spindle pole body in the methylotrophic yeast ogataea polymorpha. *Elife* **6**:1–28. doi:10.7554/eLife.24340
Marjoram RJ, Lessey EC, Burridge K. 2014. Regulation of RhoA Activity by Adhesion Molecules and Mechanotransduction. *Curr Mol Med* **14**:199–208. doi:10.2174/1566524014666140128104541
Matsui T, Maeda M, Doi Y, Yonemura S, Amano M, Kaibuchi K, Tsukita Sachiko, Tsukita Shoichiro. 1998. Rho-kinase phosphorylates COOH-terminal threonines of ezrin/radixin/moesin (ERM) proteins and regulates their head-to-tail association. *J Cell Biol*

140:647–657. doi:10.1083/jcb.140.3.647
Matsui T, Yonemura S, Tsukita SS, Tsukita SS. 1999. Activation of ERM proteins in vivo by Rho involves phosphatidylinositol 4-phosphate 5-kinase and not ROCK kinases. *Curr Biol* **9**:1259–1262. doi:10.1016/s0960-9822(99)80508-9
McCormack J, Welsh NJ, Braga VMM. 2013. Cycling around cell-cell adhesion with rho GTPase regulators. *J Cell Sci*. doi:10.1242/jcs.097923
Meenderink LM, Gaeta IM, Postema MM, Cencer CS, Chinowsky CR, Krystofiak ES, Millis BA, Tyska MJ. 2019. Actin Dynamics Drive Microvillar Motility and Clustering during Brush Border Assembly. *Dev Cell* **50**:545-556.e4. doi:10.1016/j.devcel.2019.07.008
Oshiro N, Fukata Y, Kaibuchi K. 1998. Phosphorylation of moesin by Rho-associated kinase (Rho-kinase) plays a crucial role in the formation of microvilli-like structures. *J Biol Chem* **273**:34663–34666. doi:10.1074/jbc.273.52.34663
Pakkanen R, Hedman K, Turunen O. 1987. Microvillus-specific M 75,000 plasma membrane protein of human choriocarcinoma cells. *J Histochem Cytochem* **35**:809–816. doi:10.1177/35.8.3298422
Pearson MA, Reczek D, Bretscher A, Karplus PA. 2000. Structure of the ERM protein moesin reveals the FERM domain fold masked by an extended actin binding tail domain. *Cell* **101**:259–270. doi:10.1016/S0092-8674(00)80836-3
Pelaseyed T, Bretscher A. 2018. Regulation of actin-based apical structures on epithelial cells. *J Cell Sci* **131**:jcs221853. doi:10.1242/jcs.221853
Pelaseyed T, Sauvanet C, Viswanatha R, Filter JJ, Goldberg ML, Bretscher A. 2017. Ezrin activation by LOK phosphorylation involves a PIP2-dependent wedge mechanism. *Elife* **6**:1–18. doi:10.7554/eLife.22759
Polosello C, Delon I, Valenti P, Ferrer P, Payre F. 2002. Dmoesin controls actin-based cell shape and polarity during Drosophila melanogaster oogenesis. *Nat Cell Biol* **4**:782–789. doi:10.1038/ncb856
Ratheesh A, Gomez GA, Priya R, Verma S, Kovacs EM, Jiang K, Brown NH, Akhmanova A, Stehbens SJ, Yap AS. 2012. Centralspindlin and alpha-catenin regulate Rho signalling at the epithelial zonula adherens. *Nat Cell Biol* **14**:818–828. doi:10.1038/ncb2532
Reczek D, Berryman M, Bretscher A. 1997. Identification of EPB50: A PDZ-containing phosphoprotein that associates with members of the ezrin-radixin-moesin family. *J Cell Biol* **139**:169–179. doi:10.1083/jcb.139.1.169
Reyes CC, Jin M, Breznau EB, Espino R, Delgado-Gonzalo R, Goryachev AB, Miller AL. 2014. Anillin regulates cell-cell junction integrity by organizing junctional accumulation of Rho-GTP and actomyosin. *Curr Biol* **24**:1263–1270. doi:10.1016/j.cub.2014.04.021
Rodriguez-Boulan E, Macara IG. 2014. Organization and execution of the epithelial polarity programme. *Nat Rev Mol Cell Biol* **15**:225–242. doi:10.1038/nrm3775
Sanjana NE, Shalem O, Zhang F. 2014. Improved vectors and genome-wide libraries for CRISPR screening. *Nat Methods*. doi:10.1038/nmeth.3047
Sanson M, Marineau C, Desmaze C, Lutchman M, Ruttledge M, Baron C, Narod S, Delattre O, Lenoir G, Thomas G, Aurlas A, Rouleau GA. 1993. Germline deletion in a neurofibromatosis type 2 kindred inactivates the NF2 gene and a candidate meningioma locus. *Hum Mol Genet* **2**:1215–1220. doi:10.1093/hmg/2.8.1215
Saotome I, Curto M, McClatchey AI. 2004. Ezrin is essential for epithelial organization and villus morphogenesis in the developing intestine. *Dev Cell* **6**:855–864. doi:10.1016/j.devcel.2004.05.007
Sauvanet C., Garbett D, Bretscher A. 2015. The function and dynamics of the apical scaffolding protein E3KARP are regulated by cell-cycle phosphorylation. *Mol Biol Cell* **26**:3615–3627. doi:10.1091/mbc.E15-07-0498
Sauvanet Cécile, Wayt J, Pelaseyed T, Bretscher A. 2015. Structure, Regulation, and Functional Diversity of Microvilli on the Apical Domain of Epithelial Cells. *Annu Rev Cell*

Dev Biol **31**:593–621. doi:10.1146/annurev-cellbio-100814-125234
Shalem O, Sanjana NE, Hartenian E, Shi X, Scott DA, Mikkelsen TS, Heckl D, Ebert BL, Root DE, Doench JG, Zhang F. 2014. Genome-scale CRISPR-Cas9 knockout screening in human cells. *Science (80-)* **343**:84–87. doi:10.1126/science.1247005
Speck O, Hughes SC, Noren NK, Kulikauskas RM, Fehon RG. 2003. Moesin functions antagonistically to the Rho pathway to maintain epithelial integrity. *Nature* **421**:83–87. doi:10.1038/nature01295
ten Klooster JP, Jansen M, Yuan J, Oorschot V, Begthel H, Di Giacomo V, Colland F, de Koning J, Maurice MM, Hornbeck P, Clevers H. 2009. Mst4 and Ezrin Induce Brush Borders Downstream of the Lkb1/Strad/Mo25 Polarization Complex. *Dev Cell* **16**:551–562. doi:10.1016/j.devcel.2009.01.016
Terry SJ, Zihni C, Elbediwy A, Vitiello E, San IVLC, Balda MS, Matter K. 2011. Spatially restricted activation of RhoA signalling at epithelial junctions by p114RhoGEF drives junction formation and morphogenesis. *Nat Cell Biol* **13**:159–166. doi:10.1038/ncb2156
Trofatter JA, MacCollin MM, Rutter JL, Murrell JR, Duyao MP, Parry DM, Eldridge R, Kley N, Menon AG, Pulaski K, Haase VH, Ambrose CM, Munroe D, Bove C, Haines JL, Martuza RL, MacDonald ME, Seizinger BR, Short MP, Buckler AJ, Gusella JF. 1993. A novel moesin-, ezrin-, radixin-like gene is a candidate for the neurofibromatosis 2 tumor suppressor. *Cell* **72**:791–800. doi:10.1016/0092-8674(93)90406-G
Turunen O, Wahlström T, Vaheri A. 1994. Ezrin has a COOH-terminal actin-binding site that is conserved in the ezrin protein family. *J Cell Biol* **126**:1445–1453. doi:10.1083/jcb.126.6.1445
Velasco G, Armstrong C, Morrice N, Frame S, Cohen P. 2002. Phosphorylation of the regulatory subunit of smooth muscle protein phosphatase 1M at Thr850 induces its dissociation from myosin. *FEBS Lett* **527**:101–104. doi:10.1016/S0014-5793(02)03175-7
Viswanatha R, Ohouo PY, Smolka MB, Bretscher A. 2012. Local phosphocycling mediated by LOK/SLK restricts ezrin function to the apical aspect of epithelial cells. *J Cell Biol* **199**:969–984. doi:10.1083/jcb.201207047
Wakatsuki T, Schwab B, Thompson NC, Elson EL. 2001. Effects of cytochalasin D and latrunculin B on mechanical properties of cells. *J Cell Sci* **114**:1025 LP – 1036.
Yang N, Higuchi O, Ohashi K, Nagata K, Wada A, Kangawa K, Nishida E, Mizuno K. 1998. Cofilin phosphorylation by LIM-kinase 1 and its role in Rac-mediated actin reorganization. *Nature* **393**:809–812. doi:10.1038/31735
Zihni C, Balda MS, Matter K. 2014. Signalling at tight junctions during epithelial differentiation and microbial pathogenesis. *J Cell Sci* **127**:3401–3413. doi:10.1242/jcs.145029